

Characteristics of individual surface waves measured by moored buoys in the coastal waters of the eastern Arabian Sea

Sanil Kumar V*, Sourav Mandal

Ocean Engineering, CSIR-National Institute of Oceanography
(Council of Scientific & Industrial Research), Dona Paula, Goa - 403 004 India

*Corresponding author Tel: 0091 832 2450 327 email: sanil@nio.org

Abstract

In this study, the characteristics of the individual surface waves in the eastern Arabian Sea over one year are examined based on the measured time-series data using Waverider buoys at four locations covering ~500 km of the western Indian coastline. At all locations, the number of waves is high during the non-monsoon compared to the monsoon period (June-September). Number of waves in a year is higher in the northern location (~6417657) than in the southern locations (~5497168) since comparatively more short-period waves are observed in the north. Maximum wave height varied from 7.0 to 7.6 m, and the steepness of the largest waves varies from 0.056 to 0.082 at different locations and is much smaller than the wave breaking limit. Number of short-period waves observed is higher than the long-period waves at all locations except in the monsoon, when a significant number of intermediate-period waves are present. The mean wave steepness of the 30-minutes record is ~22% higher than the conventionally reported significant wave steepness based on mean wave period. Hilbert–Huang transform method is used to detect the freak wave and analyze the abnormal wave group structure. It is observed that freak wave occurrence is high during the monsoon.

Key words: Surface waves, maximum wave height, north Indian Ocean, wave steepness, zero-up-crossing analysis

1. Introduction

Ocean surface waves (hereinafter waves) play a major role in coastal and offshore operations (Tucker and Pitt, 2001). Observation from buoys provides reliable observations of waves. Still, information on waves is obtained chiefly through satellite-based altimeter measurements or model datasets since the direct observations from the buoys are sparse and the spatial availability of the data is limited (Cavaleri and Sclavo, 2006). Studies using satellite altimeter or model data typically describe the wave field using the significant wave height (H_s), mean wave period and/or spectral peak period (Semedo et al., 2011; Vinoth and Young, 2011; Kumar et al., 2013; Hithin et al., 2015; Sandhya et al., 2014; Amrutha et al., 2016a). Nonetheless, for practical applications, information on the height, length and steepness of individual waves at a given place during a specific duration might be necessary (DNV, 2010).

One example of an application benefiting from the information of single waves is the tuning of wave energy converters (WEC's). At present many of these WECs are tuned to peak spectra frequency for enhancing heaving motion. Retuning the devices to each individual wave rather than peak spectra frequency, will significantly increase the energy conversion rate (Smith et al., 2006). However, the extent to which the WEC can be retuned, depends on the design of the device and the rate of change of wave period between two successive incoming individual waves. In the real ocean, due to nonlinearity, a higher number of individual waves may lead to a higher rate of change of wave period, which adds more complexities to the design development of WEC. Hence, information on the number of individual waves for one-year period will help in the selection of wave energy farming sites. Also, each individual wave induces wave load fluctuations to the components of offshore WEC, wind farms, jack-up platforms. The compound effect of these individual fluctuations can ultimately lead to fatigue.

Wave steepness (δ) is the ratio between height and length of a wave and indicates wave stability, with steeper waves representing greater marine hazard. As the surface gravity waves approach the coastal waters, wave height increases, the wavelength decreases, and δ increases. When δ reaches the Stokes limit of $0.1428 \tanh(kd)$, the wave becomes unstable and breaks (Stokes, 1880). The steepness of a sea state is important to evaluate the loading on floating structures which tends to be higher in steep sea states (Bitner-Gregersen et al., 1998). High wave steepness coupled with high wave height forms a severe sea state and poses a problem to the navigation of the vessels and boats (Fonseca and Guedes Soares, 2003). Analysis of the global ship accident database from January 1995 to April 1999 indicates that more than 50% of the accidents happened when the δ was more than 0.035 (Toffoli et al., 2005). Smaller vessels capsize when the δ increases in the coastal regions. Kraus and

Larson (1988) reported that δ plays an important role in beach erosion and accretion. Generally, linear wave relationships are valid if the δ is less than 0.01. As δ increases, higher-order models such as the 5th order Stokes waves are more accurate (Dean and Dalrymple, 1991). The run-up height on an offshore structure is a function of the wave steepness and the wave height to diameter ratio (DNV, 2010). Hence, it is necessary to understand the steepness of individual waves in the ocean, especially high waves.

Most of the earlier studies on steepness described the integral wave steepness or the spectral wave steepness estimated based on H_s and either mean wave period or peak wave period (Taylor and Yelland, 2001). In most cases, the H_s is based on the statistics of waves measured for 20 or 30 minutes. H_s and mean wave period are estimated either from zero-up-crossing analysis (Tucker, 1991) of the time-series data or the wave spectrum. Nowadays, the data on the height and period of individual waves are available from almost all instrumented measurements.

Arabian Sea (AS) is an area where the monsoon winds are a dominant feature, and it reverses their direction in different seasons over an annual cycle (Schott and McCreary, 2001). South-westerly (SW) winds prevail from May to September for summer monsoon and north-easterly (NE) from November to February for the winter season. The wave heights in AS reach higher values during the monsoon period (June-September) than the remaining period due to the strong southwesterly winds prevailing over the AS (Kumar et al., 2014). The earlier studies in the eastern AS indicate the presence of long-period waves from south and southwest superimposed to the wind-seas from west and northwest (Kumar et al., 2014; Anjali Nair and Kumar, 2016, 2017; Glejin et al., 2016). Mainly, three different wave systems reach the eastern Arabian Sea. The first is characterized by southerly swells generated in the Indian Ocean (Amrutha and Kumar, 2021), the second is the energetic monsoon waves (Kumar et al., 2000) from the west due to Somali jet (Findlater, 1969), and the third is the northwesterly waves generated due to *shamal* and *makran* winds (Aboobacker et al., 2011; Anoop et al., 2015).

The studies mentioned above focused on understanding the bulk wave characteristics along the eastern AS and did not focus on the variability of wave steepness and the characteristics of individual waves. In this study, the height and steepness of individual waves measured over one year simultaneously at four locations covering ~500 km along the eastern AS are examined and are used to describe its spatial and temporal variations. The characteristics of the steepness of the measured high waves are also examined. This study is based on the continuously measured wave buoy data covering one year at each location. The rest of the paper is structured as follows. Data and methods are described

in Section 2. Section 3 covers the results and discussions, and Section 4 summarizes and concludes the study.

2. Data and method

2.1 Data

The measured wave data using the moored 0.9 m diameter Datawell Directional Waverider-MkIII buoy (Datawell, 2009) from 1 January 2017 to 31 December 2017 at 4 locations along the eastern AS are used in the study (Figure 1). Table 1 provides an overview of the positions of the measurement locations and the water depth at each position. The distance between Versova (northernmost location) and Ratnagiri is ~230 km, Ratnagiri and Vengurla is ~130 km and Vengurla – Karwar (southernmost location) is ~ 140 km. The buoy data sampled at a rate of 3.84 Hz but logged at a sampling frequency of 1.28 Hz, and there is no data gap for the period selected (Table 1). The Waverider buoy measures the vertical and horizontal acceleration of the sea surface. Heave is measured with 3% accuracy and 1 cm resolution. The water depth at the measurement locations varied from 10 to 15 m with respect to chart datum (Table 1). The variation in water depth due to tide is not taken into account in the analysis. The mean spring tidal range varies from 1.58 to 3.66 m from south to north along the study area. The height (H) and period (T) of the individual waves are obtained from the zero-up-crossing method (Tucker, 1991). Wavelength (L) is estimated from the wave period and the water depth by iteratively solving the wave dispersion relation. Significant wave height ($H_{1/3}$) and significant wave period ($T_{1/3}$) are obtained from the individual wave parameters in a 30-minutes record. The maximum height of the wave in a 30-minutes duration is maximum wave height (H_{max}). The wave spectrum of surface elevation is estimated from the measured heave data at every 30-minutes through Fast Fourier Transform (FFT). The wave spectrum is with a resolution of 0.005 Hz from 0.025 Hz to 0.1 Hz and after that, it is 0.01 Hz up to 0.58 Hz (Datawell, 2009). Significant wave steepness is estimated from the H_s and mean wave period (T_{m02}) obtained from the wave spectrum. The average wave period ($T_{m-1,1}$) and energy wave period ($T_{m-1,0}$) are estimated from the spectral moments. The spectral width parameter (ν) (Longuet-Higgins, 1975) can be an indicator of the strength of non-linear focusing and it is calculated from the moments of the spectrum and it varies from 0 to 1 with lower values for narrowband spectrum, i.e., the energy is concentrated near the spectral peak frequency, as individual waves have similar frequency with differing amplitudes. The notations used and the details of the parameters are given in Annexure. The measured individual waves are classified into 3 groups following Bromirski et al. (2015), i) short-period (SP) waves ($T < 6$ s), is dominated by wind-seas, ii)

long-period (LP) waves ($T > 8$ s), results primarily from swell and iii) intermediate-period (IP) waves ($6 \text{ s} \leq T \leq 8 \text{ s}$).

The interannual variations in the height, period, length and steepness of individual waves from 1 June to 31 July during 2010 to 2019 are examined based on the mean, 99 and 90 percentile values from the measured wave data at Ratnagiri.

In order to estimate the δ , the data on the wavelength at the buoy location is obtained iteratively considering the water depth at the buoy location following the linear dispersion relation from the period of the wave (Goda, 2010). The 99 and 95 percentile wave steepness and wave height are computed from the half-hourly time series. The different percentile lines (e.g., 99 percentile) indicate how often the wave steepness/height is below a particular value (e.g., 99%) in that record. Buoy measurements are in Coordinated Universal Time (UTC) and the local time is 05:30 h ahead of UTC.

Waves with a length less than half the water depth are classified as deep-water waves, while those with a length more than $1/20^{\text{th}}$ of water depth are classified as shallow-water waves and the rest as intermediate water waves (Holthuijsen, 2007).

Waves higher than expected for a given sea state are commonly referred to as freak waves (Bitner-Gregersen and Gramstad, 2016). One of the criteria to identify a freak wave is that its wave height is more than twice the H_s of the surrounding seas (Haver, 2001) and is used in the present study.

2.2 Bivariate probability density

A continuous distribution gives the more precise statistical information about random waves for a given sea state than an empirical distribution based on a set of measured waves. A probability density of five-parameter bivariate gamma distribution is adopted and measured wave height and steepness data are fitted into this. Then, theoretical fits are compared with the bivariate empirical density. In order to fit the measured wave height and steepness data into theoretical density, normalized wave height (H^*) and normalized wave steepness (δ^*) are used and they are defined by $H^* = \frac{H}{\sqrt{m_0}}$ and $\delta^* = \delta \frac{L_m}{H_m}$ with m_0 , L_m , H_m being the zero moment of the wave spectrum, mean wavelength and mean wave height for a particular wave record. In the present work, Smith, Aldelfang and Tubbs' five-parameter bivariate gamma density function (Smith et al., 1982) is adopted.

$$f(x, y) = \frac{G_1(x, y)}{G_2} + \sum_{i=0}^{\infty} \sum_{j=0}^{\infty} g_{ij} x^i y^{i+j}, \quad (1)$$

Where $G_1(x, y) = x^{\alpha_x - 1} y^{\alpha_y - 1} e^{\left(\frac{-x+y}{1-\eta}\right)}$, $G_2 = (1 - \eta)^{\alpha_x} \Gamma(\alpha_x) \Gamma(\alpha_y - \alpha_x)$, and

$$g_{ij} = \frac{\eta^{i+j} \Gamma(\alpha_y - \alpha_x + j)}{(1-\eta)^{2i+j} \Gamma(\alpha_y + i + j) i! j!}, \quad \eta = \rho \sqrt{\frac{\alpha_y}{\alpha_x}}$$

In equation (1), $x = X\beta_X$ and $y = Y\beta_Y$ where β_X, β_Y are the scale parameters and α_X, α_Y are the shape parameters and ρ which is the correlation coefficient between X and Y , bounded as $\eta \sqrt{\frac{\alpha_x}{\alpha_y}} \geq \rho \geq 0$. To fit the empirical density of measured normalized wave height (H^*) and normalized wave steepness (δ^*) in theoretical density as in equation (1), $\alpha_X, \alpha_Y, \beta_X,$ and β_Y are estimated with the method of moments (Antão and Soares, 2016).

$\alpha_X = \frac{M_X^2}{S_X^2}, \alpha_Y = \frac{M_Y^2}{S_Y^2}, \beta_X = \frac{M_X}{S_X^2},$ and $\beta_Y = \frac{M_Y}{S_Y^2}$ where M and S are the mean and standard deviation of sample data sets.

2.3 Hilbert-Huang Transform Method

The record containing one freak wave signal (A2 02:56 h) on 31 May 2017, one record before (A1 02:26 h) and one record after (A3 03:26 h) at Ratnagiri is examined to understand the localized characteristics of freak wave in the time-frequency domain using Hilbert-Huang transform (HHT) method. The detailed procedure of HHT method and its performance over several Fourier-based methods for non-stationary and non-linear time series, can be found in Huang et al. (1998). HHT method mainly decomposes non-stationary and non-linear time series into several sub-signals, namely Intrinsic mode functions (IMF) using Empirical Mode Decomposition (EMD) methods. While deriving IMFs, the two conditions are applied: (a) the number of zero-crossings and local extreme points must be either equal or differ by at most one and (b) the mean of the envelopes which is defined by the local maxima and minima must be zero at any point. A bandpass filter can be employed in pre-processing to reduce the input signal into a narrow band sub-signal for EMD shifting. This method solves the inherent mode mixing problem in HHT to a great extent (Bao et al. 2009). If $C_k(t)$ s is the n number of IMFs extracted from a wave record $X(t)$, the associated error due to reconstruction can be expressed as $(X(t) - \sum_{k=1}^n C_k(t) + Residual)$, where $X(t)$ is the wave record. After decomposition, using Cauchy principal value, following Hilbert transform is applied to each IMFs in order to derive the instantons energy skeleton of the signal

$$H_k(t) = \frac{1}{\pi} \int_{-\infty}^{\infty} \frac{C_k(\tau)}{t-\tau} d\tau \quad (2)$$

The associated analytical signal $Z_k(t)$ can be expressed as $Z_k(t) = C_k(t) + iH_k(t) = a_k(t)e^{i\theta_k t}$, where $a_k(t) = \sqrt{C_k^2 + H_k^2}$ and $\theta_k = \tan^{-1}\left(\frac{H_k}{C_k}\right)$. The instantaneous frequency ($\omega_k(t)$) and energy ($IE(t)$) can be determined by the following relations:

$$\omega_k(t) = \frac{d\theta_k(t)}{dt} \text{ and } IE(t) = \int_{\omega} H^2(\omega, t)d\omega.$$

3. Results and discussions

3.1 Wave height and period

The wave heights in coastal waters of eastern AS largely vary with seasons, and most energetic waves are during June-September due to the prevailing monsoon, and relatively calm conditions prevail during the remaining months (Figure 2a-d). Earlier studies also indicated that the waves in the study area are high during June and July due to the strong winds generated by the Asian summer monsoon (Kumar et al., 2014). Slightly higher wave heights are observed on 4 and 5 December 2017 due to the influence of tropical cyclone Ockhi. Along the coast, the distribution of wave height is similar (Figure 3a). Heights of individual waves are slightly higher with an annual mean value of 0.62 m in the southernmost location than in the northernmost location (annual mean value of 0.49 m).

The significant wave height estimated from the wave spectrum (H_s) is always higher than that estimated based on zero-up-crossing analysis ($H_{1/3}$) for deep-water waves (Figure 4a-d) and on an average, H_s is 1.17 times $H_{1/3}$. For narrow-banded processes, the H_s is equivalent $H_{1/3}$ (Goda, 1970). In the study area, the annual mean H_s varied from 0.91 to 1.14 m and the annual mean H_{\max} varied from 1.38 to 1.76 m (Table 1). The annual maximum wave height varied from 5.7 to 7.6 m along the coast, with the highest value in the southern location, and the values decreased towards the north, while the H_s reached up to 3.6 to 4.0 m among the locations. But the number of waves with a height more than 5 m is maximum (517) at Ratnagiri, followed by Karwar (442), Vengurla (189) and Versova (45). The 99th percentile value of individual wave height has a maximum value of 5.0 to 5.8 m at the locations studied, while the 95th percentile value is 3.9 to 4.8 m (Figure 2a-d). In the non-monsoon period, the maximum wave height measured is 3.5, 4.8, 4.4 and 5.0 m at Versova, Ratnagiri, Vengurla and Karwar and these values are measured in May (Table 2). The maximum wave height during the cyclone Ockhi is 3.8 to 4.8 m and is less than that during the monsoon period.

The crest heights of the maximum wave in a 30-minute record vary from 0.39 to 0.74 times the wave height with an average value of 0.6. For waves with height more than 5 m, the crest height is 0.36 to 0.75 times the wave height with an average value of 0.6. Since the waves are measured in the nearshore waters, the crest height is more than the trough height for high waves. 36, 36.4, 42.2 and 39.6% of the measured waves fall in deep-water waves at locations Versova, Ratnagiri, Vengurla and Karwar, while the balance is under intermediate water waves, except at the northern location, where 0.01% of waves are in shallow-water waves.

In the design of coastal structures, significant wave period ($T_{1/3}$) from the zero-crossing analysis is used (Goda, 2010). The $T_{1/3}$ has higher values compared to the mean wave period (T_{m02}) obtained from the wave spectrum (Figure 4e-h). At the same time, the significant wave period compares well with the average wave period ($T_{m-1,1}$) for all locations with correlation coefficient of 0.88 to 0.94 (Figure 4i-l). Energy wave period ($T_{m-1,0}$) comparison with significant wave period indicates that the $T_{m-1,0}$ is higher than $T_{1/3}$ with a positive bias of 0.8 to 0.9 s (Figure 4m-p). Chun and Suh (2018) reported that $T_{m-1,0}$ compares well with $T_{1/3}$ for waves in East Sea of Japan, while for the present study area, $T_{m-1,1}$ compares well with $T_{1/3}$. T_{m02} is underestimated compared to $T_{1/3}$ when nonlinearity increases due to overestimation of the second-order moment m_2 due to the presence of the non-linear spectral components.

The distribution of wave period is different along the locations studied (Figure 3b). 45% of the waves in the northern location are shorter than 4.0 s, whereas, in the southern location, 32% of waves are shorter than 4.0 s. Wavelength is less than 30 m during 55% of the time in the northern location, while it is 40% in the southern location (Figure 3c). The monthly average value of the mean wave period ranges from 4.5 to 7.5 s except in the northern location, where slightly lower wave periods are observed (4.0 to 7.0 s). The number of waves is high during the non-monsoon months compared to that during the monsoon months since the mean wave period is larger during the monsoon months than the rest of the year (Figures 5a and 4c). The number of waves in a year is much higher in the northern location (~6417657) compared to the southern locations (~5497168) since in the northern location large number of short-period waves is observed, resulting in a lower mean wave period, whereas in the southern location mean wave period is high (Figure 5c). The annual mean wave period is 4.8, 5.3, 5.5 and 5.6 s for locations from north to south. Half of the records showed a period shorter than 4.2 s in the northern location and 5.1 s in the southern location and 25% of them are higher than 5.9 s and 7.2 s in the north and south. The period of waves with height more than 5 m varied from 6.6 to 13.8 with a mean value of 10.0 s. The monthly average wave heights indicate that wave heights are slightly higher in the southern location except in July. In July, wave heights are highest at Ratnagiri. The monthly mean wave height in June, July, and August is ~3 times the value in January to April (Figure 5b). The values of the mean wave period are generally higher in the monsoon (Figure 5c).

Seasonally there is a large variation in the direction of the waves (Figure 6). During the pre-monsoon (February-May), waves are mostly from the northwest in the northern location, but they are from the south-west in the southern location, indicating a spatial variation in wave direction. Along the eastern Arabian Sea, the number of northwest waves reduces from north to south (Figure 6). Earlier

studies indicated that the northwest waves are mainly due to *shamal* winds (Aboobacker et al., 2011) and winds in the *Makran* region (Anoop et al., 2020).

3.2 Wave steepness

At all locations, the wave steepness (δ) is less than the wave breaking limit, except for a few small waves with a height less than 1 m and a period less than 3 s (Figure 2e-h). The mean value of wave steepness in the 30-minute record varied from 0.003 to 0.038, while the maximum values varied from 0.010 to 0.205. Even though the maximum wave steepness exceeded the limiting value of 0.1428, the 99th percentile value was within the limiting value. 99th percentile value varied from 0.008 to 0.118 (Figure 2e-h). 90th percentile value varied from 0.006 to 0.084.

Locations with average δ more than 0.015 are preferred for installing wave energy converters (WEC) as the performance of WECs is significantly higher in steep waves (Pecher and Kofoed, 2017). The wave steepness is more than 0.015 during 47, 46.2, 36 and 43% of the times at Versova, Ratnagiri, Vengurla and Karwar.

The maximum value of steepness of H_{\max} observed are 0.119, 0.091, 0.106, and 0.113 at Versova, Ratnagiri, Vengurla and Karwar and all are with wave height < 1.5 m. Among the locations studied, the longest wave during 2017 is recorded at Ratnagiri with a wavelength of 250 m and had a height of 0.8 m. At other locations, the maximum wavelength varied from 223 to 231 m and was with height varying from 0.6 to 1.6 m. The steepness of the longest wave at different locations varied from 0.003 to 0.007. The steepness of the highest waves varied from 0.057 to 0.082, with the highest value in the southern location and the lowest value in the northern location, similar to the spatial distribution of H_{\max} . The steepness of the waves with height more than 5 m varied from 0.025 to 0.097 with an average value of 0.052.

Wave steepness decrease as the wave period increase for a given value of height and it increases as height increases for a given value of the period. Wave steepness strongly depends on the wave period since it is inversely proportional to the square of the wave period. High wave steepness is observed even for waves with height less than 2 m. But for waves with period more than 4 s, the maximum wave steepness is 0.118, which is less than the breaking limit. Waves with period more than 4 s formed 63% of the data along the study region. For waves with period more than 5 s, the maximum wave steepness is 0.104. Thompson et al. (1984) grouped ocean waves as locally generated waves, if the steepness values are greater than 0.025. For the study area, average period and height of waves are 3.2-3.9 s and 0.6-0.9 m when the steepness is more than 0.025. 20, 18.5, 14 and 17.8% of the waves

are with δ more than 0.025 at Versova, Ratnagiri, Vengurla and Karwar, respectively (Figure 3d). Annually, only 1% of the waves had steepness more than 0.053.

The temporal distribution of wave steepness in a day indicates that the maximum steepness is mostly from 0900 to 1500 UTC in the non-monsoon, while during the monsoon, such a pattern is not observed (Figure 7). Earlier studies indicate that along the eastern Arabian Sea, wind-seas increase during 0900 UTC and reach the peak at 1300 UTC due to the sea breeze (Amrutha et al., 2016b). The increase in the average wave steepness in the non-monsoon is due to the presence of large number of short-period waves during this period.

Seasonal variation in wave steepness is examined with monthly mean values (Figure 5d). At all locations, monthly mean wave steepness is high in July, similar to the variation in monthly mean wave height (Figure 5b). In most of the months, the wave steepness is high at Versova compared to other locations, except in June, July and December. Seasonal average wave steepness is also highest at Versova in all seasons, followed by Ratnagiri.

Since most of the earlier studies discussed the significant wave steepness (δ_m) based on significant wave height and mean wave period, it is computed and compared with the mean steepness ($\langle\delta\rangle$) of the waves recorded in a 30-minutes record (Figure 8). The comparison shows that $\langle\delta\rangle$ is higher than the δ_m for all the locations studied and $\langle\delta\rangle$ is ~ 1.19 to 1.22 times the δ_m . The maximum values of δ_m at the study locations is 0.033, 0.033, 0.031 and 0.033 at Versova, Ratnagiri, Vengurla and Karwar (Figure 8). Significant wave steepness (δ_p) based on T_p shows a larger scatter when compared to the mean wave steepness (Figure 8), which indicates the importance of considering the steepness of individual waves in the design calculations. The maximum values of δ_p at the study locations are 0.071, 0.048, 0.059 and 0.055 at Versova, Ratnagiri, Vengurla, and Karwar (Figure 8).

The maximum value of δ_m to be considered in the design calculation of marine structures for high sea states as per DNV Rules (DNV 2000) is $1/15$ (0.067). The maximum value of δ_m in the present study area is 0.033. In the Norwegian Continental Shelf, significant steepness is in the range $1/15 - 1/14.3$ (Bitner-Gregersen et al., 1998). In the deep waters of the Norwegian continental shelf, the mean values of the wave steepness of wind-sea are in the range 0.031-0.046 and for combined swell and wind-sea, the values are in a wider range 0.0054-0.125 (Myrhaug, 2018). The average value of δ_m in the deep waters of Portugal is ~ 0.031 (Mendes and Oliveira, 2021). The average value of the δ_m in the coastal waters of eastern AS at 15 m water depth is ~ 0.025 .

Variation of $\langle \delta \rangle$ with significant wave height, peak wave period and mean wave period is presented in Figure 9. As expected $\langle \delta \rangle$ increases with increase in H_s , but shows wide scatter with T_p and T_{m02} .

3.3 Interannual variations in wave steepness

Interannual variations in 99 percentile height are up to 11.7%. The average height for June-July is minimum (1.26 m) in 2019 and maximum (1.51 m) in 2013, with interannual variations up to 11.6% (Figure 10). The average value of the wave period ranges from 6.6 to 7.1 s. The variations in wavelength are up to 4.8% for 99 percentile and are 5.8% in average value. The mean value of wave steepness varied from 0.022 to 0.027, while the 99 percentile values varied from 0.063 to 0.074, with interannual variation up to 9.4%. 90 percentile value of steepness varied from 0.037 to 0.044.

3.4 Bivariate probability density for height and steepness

In Figure 11, the bivariate empirical probability density is compared with theoretical probability density for three different wave records from Ratnagiri. The plots are presented for different spectral width parameter (0.51, 0.60 and 0.70). The peak of fitted theoretical density is observed at the area of lower height and steepness than that of empirical density, which may be due to the assumption of small amplitude water wave theory while calculating wavelength. This phenomenon is also observed in the case of joint probability density fit of wave height and steepness based on the Longuet-Higgins formula (see Longuet-Higgins, 1983; Antão and Guedes Soares, 2015). The theoretical fit overestimates the peak density. However, the interval around the peak density matches quite well between theoretical density and empirical density. The maximum value of the empirical density (maxE) and maximum value of the theoretical density (maxT) are in reasonable agreement. However, the theoretical density slightly underestimates the probabilities of waves of low steepness and low height area. Larger values of spectral width parameter imply a broad-banded spectrum. With the increase of spectral width parameter, the correlation (= 0.45, 0.36, 0.05 for plot (a), (b) and (c) respectively) between the wave height and steepness decreases and better agreement between theoretical and the empirical density is observed.

3.5 Short, intermediate and long-period waves

In each location, the number of short-period ($T < 6$ s), long-period ($T > 8$ s), and intermediate-period waves ($6 \text{ s} \leq T \leq 8 \text{ s}$) in the 30-minutes measured record during different seasons are examined. In the fair-weather (February-May), short-period waves were 82.5, 75.1, 72.1, and 68.8% at locations from north to south (Figure 12). While in the southwest monsoon (June-September), short-period wave

occurrence reduced to 53.2, 44.7, 40.9, and 41.1% (Table 3). During the post-monsoon (October-January), the percentage of short-period waves is 80.6, 76.0, 68.3, and 69.0, somewhat similar to that during the fair-weather period. Compared to other seasons, intermediate-period waves are common during the southwest monsoon, with the occurrence of 19.6, 23.9, 22.8, and 23.6% at Versova, Ratnagiri, Vengurla and Karwar. During the southwest monsoon, percentage of long-period waves are also more than those in other seasons, with the occurrence of 27.2, 31.4, 36.3, and 35.3%. Annually 72% of waves are short-period waves in the northern location and it reduces to 59.6% in the southern location, while long-period waves and intermediate-period waves increase from north to south. Even though there are significant changes in the percentage of short-period and long-period waves among the locations studied, the variations in the annual mean value of spectral peak period are minimum with values of 10.0, 10.4, 11.4 and 11.2 s at Versova, Ratnagiri, Vengurla and Karwar.

A higher relative number of short-period waves coincides with a more narrow banded spectrum (Figure 13). When combined sea states consisting of long-period and short-period waves are present, the spectral width parameters have high value indicating a broad-banded spectrum.

Although the number of short-period waves is high during the non-monsoon period, the heights of long-period waves are higher than the short-period waves in all seasons (Table 3). Also, the intermediate-period wave heights are higher than the short-period waves and lower than the long-period wave heights (Figure 12). The mean values of the wave steepness during the short-period waves dominated sea states are in the range 0.010-0.038 and that during the long-period waves dominated sea states are in the range 0.005-0.029.

3.6 Freak waves

The abnormality index, i.e., the H_{\max} to H_s ratio, varied from 1.3 to 2.6, with a mean value of 1.67 to 1.68 at different locations. When H_{\max} is more than two times the corresponding H_s , the wave is called freak waves (Mori and Janssen, 2006). When large waves attain high steepness, freak waves are formed and are an important characteristic of a severe sea state. On average, during the southwest monsoon, freak waves are observed in 3.0 to 3.5% of the 30-minutes record in the study area, with the maximum at Ratnagiri (Figure 14). Freak waves are also observed during the non-monsoon period but with wave heights less than 1 m (Figure 14). Annually, freak waves are observed in 0.8 to 1.2% of the 30-minute records. In the study locations, the freak waves varied from 138 to 212 in 17520 data, i.e., 1 out of 83 to 127 data. The ratio of wave height to significant wave height that is likely to be exceeded in 1 out of 100 cases is about 2.0 (Haver, 2001). In the South China Sea, from May to August, the occurrence probability of the observed freak waves is in the range of 0.03-0.53% (Xinran et al., 2022).

The six years of wave measurements from 11 sites in the southern North Sea indicate that the freak (rogue) wave frequencies are relatively constant over seasons and uncorrelated between stations (Teutsch et al., 2020). Amrutha and Kumar (2017) observed that in the nearshore waters of the eastern Arabian Sea, the H_{\max}/H_s ratio is 1.50-1.62 for different locations. No specific pattern on the occurrence of freak wave with time in a particular day could be noticed. Earlier studies based on laboratory experiments, wave models, and field data have shown that for narrow banded spectrum, freak waves occurred in sea states with δ_p more than 0.07 (Bitner-Gregersen and Gramstad, 2016). But in the present study, the significant steepness (δ_p) is less than 0.07 during the freak wave incidents and this difference is due to the fact that in the study area, the wave spectrum is broad-banded due to the combined presence of wind-seas and swells.

The time series A2 is decomposed into 9 different Intrinsic mode functions (IMF) C_k (for $k=1\dots9$) using the Empirical Mode Decomposition (EMD) technique. The instantaneous frequency (IF), energy and Hilbert energy spectrum of the wave record A2 are obtained and used for analysis. In Figure 15, the nine different IMFs and residual are presented for A2. It can be observed that different IMFs carry different ranges of energy. IMF1 is the most energetic while IMF2 is the second most dominant and they contribute most towards the reconstruction of A2. The associated error due to reconstruction is negligible. It is found that the zero-up-crossing mean IMF Period increases monotonically with the increase of IMF's ranking for A2. The occurrence of freak waves can be identified by the instant surge of energy signature at plotted energy skeleton. Figure 16(a) reveals that the high energy associated with the abnormal wave group existed at the low-frequency regime. However, the energy signature is also carried over to the higher frequency regime during the occurrence of the freak wave.

The variations of local frequencies of IMF1 and IMF2 are presented in Figure 16(b) within the vicinity of the abnormal wave group. It is observed that the variation of instantaneous frequency within the abnormal group is small for both IMF1 and IMF2. This difference between instantaneous frequency majorly contributes to the abnormal wave group profile, as discussed in Wu and Yao (2004).

The individual wave group is determined for the pre (A1) and post (A3) wave records of A2. Individual wave group is characterized by the time group length (tgl) and group energy (Egl) (see Mandal et al., 2020). Time group length is determined as the time gap between two successive uncrossing of the threshold energy level, which is the mean value of one-third of the highest instantaneous energy by the instantaneous energy. Group energy is the total instantaneous energy contained in a corresponding time group length. In Figure 16(c), the group power ratio (GPR) (Egl/tgl)

between group energy and time group length are plotted. It is observed that the number of individual wave groups for A2 is lesser than A1 and A3 while GPR is higher than A1 and A3. It can be seen that before the formation of the freak wave individual group, the significant GPR (mean of the highest 1/3 of the GPR excluding freak wave GPR) for A2 becomes higher than the significant GPR of A1. Highest GPR is observed for the individual group associated with the freak wave at A2.

The mean group length ($\overline{t_{gl}}$) is calculated from the HHT method for a one-year wave record at Ratnagiri and plotted with spectral width parameter in Figure 17. It is observed that overall mean group length increases as the spectral width becomes more wider, which may be due to the interaction between the wind-seas and swells. However, the mean time group length does not decrease beyond ~ 15 s for the sampled wave records.

4. Conclusions

The waves measured simultaneously at 4 locations in the coastal waters of the eastern Arabian Sea at 10 to 15 m water depth during 2017 indicate that 36 to 42% of the waves fall in deep water and the balance in intermediate waters. The number of short-period waves observed at all locations is higher than the long-period waves during the non-monsoon period. The significant wave height estimated from the wave spectrum is always higher than that estimated based on zero-up-crossing analysis and the significant wave period ($T_{1/3}$) shows a large deviation from the mean wave period (T_{m02}) but compares well with the average wave period ($T_{m-1,1}$) based on wave spectrum. Along the coast, there are significant changes in the wave period. Long-period waves and intermediate-period waves decrease from south to north. The steepness of the waves with height more than 5 m varied from 0.025 to 0.097 and these values are below the limiting steepness. The mean values of the wave steepness during the short-period waves dominated sea states are higher than that during the long-period waves dominated sea states. The interannual variations in wave steepness during the high waves are up to 9.4%. For more precise statistical information, a probability density of five-parameter bivariate gamma distribution is compared with empirical density of measured wave steepness and height. It is observed that the spectral width parameter is inversely proportional to the correlation values between wave steepness and height and the agreement between theoretical and empirical density increases as the correlation values decreases. The Hilbert spectrum detects the appearance of freak waves both in the time and frequency domains. Annually, freak waves are observed in 0.8 to 1.2% of the 30-minute records and the significant steepness based on peak period is less than 0.07 during the freak wave incidents. It is found that the variations of instantaneous frequency are small in abnormal wave groups for the two most dominant Intrinsic mode functions, which significantly

contribute towards the abnormal wave group profile. Mean wave steepness of 30-minute record is ~22% higher than the significant wave steepness of the same record based on mean wave period and hence, the steepness of individual high waves is to be examined before finalizing the steepness value to be considered in various design calculations.

Author Contributions:

Sanil Kumar - data analysis and original draft

Sourav Mandal -data analysis and editing

Funding: This research received no external funding.

Acknowledgments

The authors acknowledge the ESSO-Indian National Centre for Ocean Information Services (INCOIS), Ministry of Earth Sciences for funding the wave measurements at Versova, Ratnagiri and Karwar and CSIR-NIO for measurements at Vengurla. We thank TM. Balakrishnan Nair, Head OSISG, Arun Nherakkol, Scientist, INCOIS, Hyderabad, Dr Udhaba Dora, Scientist and Jai Singh, Technical Officer, CSIR-NIO for help during data collection. We thank Dr Bhaware B G, G. M. Vedak College of Science, Raigad and Dr. JL Rathod, Department of Marine Biology, Karnataka University PG Centre, Karwar for providing the logistics required for wave data collection at Ratnagiri and Karwar. We thank both the reviewers for the suggestions which improved the scientific content of this paper. This publication is a NIO contribution -----.

Conflicts of Interest: The authors declare no conflicts of interest.

References

- Aboobacker, V.M., Rashmi, R., Vethamony, P., Menon, H.B., 2011. On the dominance of pre-existing swells over wind seas along the west coast of India. *Continental Shelf Research* 31, 1701–1712. <https://doi.org/10.1016/j.csr.2011.07.010>.
- Amrutha, M.M., Kumar, V.S, Singh, J., 2016b. Changes in nearshore waves during the active sea/land breeze period off Vengurla, central west coast of India, *Annales Geophysicae* 34, 215-226 doi:10.5194/angeo-34-215-2016.
- Amrutha, M.M., Kumar, V.S., 2017. Characteristics of high monsoon wind-waves observed at multiple stations in the eastern Arabian Sea, *Ocean Science Discussions*, <https://doi.org/10.5194/os-2017-84>.
- Amrutha, M.M., Kumar, V.S., 2021. Identification of wave systems in the multimodal sea state along the Indian shelf seas, *Ocean Dynamics*, <https://doi.org/10.1007/s10236-021-01456-x>
- Amrutha, M.M., Sanil Kumar, V., Sandhya, K.G., Balakrishnan Nair, T.M., Rathod, J.L., 2016a. Wave hindcast studies using SWAN nested in WAVEWATCH III - comparison with measured nearshore buoy data off Karwar, eastern Arabian Sea, *Ocean Engineering* 119C, 114-124. [10.1016/j.oceaneng.2016.04.032](https://doi.org/10.1016/j.oceaneng.2016.04.032).
- Anjali Nair, M., Kumar, V.S., 2016. Spectral wave climatology off Ratnagiri - northeast Arabian Sea, *Natural Hazards*, 82, 1565-1588. [10.1007/s11069-016-2257-5](https://doi.org/10.1007/s11069-016-2257-5).
- Anjali Nair, M., Kumar, V.S., 2017. Wave spectral shapes in the coastal waters based on measured data off Karwar on the west coast of India, *Ocean Science*, 13, 365–378, doi:10.5194/os-13-365-2017.
- Anoop, T.R., Kumar, V.S, Shanas, P.R., Glejin, J., 2015. Surface wave climatology and its variability in the North Indian Ocean based on ERA-Interim reanalysis, *J. Atmos. Oceanic Technol.* 32(7), 1372-1385. doi.: [10.1175/JTECH-D-14-00212.1](https://doi.org/10.1175/JTECH-D-14-00212.1).
- Anoop, T.R., Shanas, P.R., Aboobacker, V.M., Kumar, V.S, Nair, L.S., Prasad, R., Reji, S., 2020. On the generation and propagation of Makran swells in the Arabian Sea, *International Journal of Climatology* 40, 585–593. doi: [10.1002/joc.6192](https://doi.org/10.1002/joc.6192)
- Antão, E.M., Soares, C.G., 2015. Joint distributions of wave steepness in narrow band sea states. *Ocean Engineering*, 101, 201-210.
- Antão, E.M., Soares, C.G., 2016. Approximation of the joint probability density of wave steepness and height with a bivariate gamma distribution. *Ocean Engineering*, 126, 402-410.
- Bao, C., Hao, H., Li, Z.X., Zhu, X., 2009. Time-varying system identification using a newly improved HHT algorithm. *Computers & Structures*, 87(23-24), 1611-1623.
- Bitner-Gregersen, E.M., Gramstad, O., 2016. Rogue waves: impact on ships and offshore structures. *Det Norske Veritas Germanischer Lloyd Strategic Research and Innovation Position Paper 5–2015*, 60 pp.

- Bitner-Gregersen, E.M., Guedes Soares, C., Silvestre, A., 1998. On the Average Wave Steepness, Proceedings of the Conference Ocean Wave Kinematics, Dynamics and Loads on Ship Structures (Wave'98), Houston, Texas, ASCE, April 30-May 1, pp 513-520 p.
- Bromirski, P. D., Cayan, D. R., Flick, R. E., 2005, Wave spectral energy variability in the northeast Pacific, *J. Geophys. Res.*, 110, C03005, doi:[10.1029/2004JC002398](https://doi.org/10.1029/2004JC002398).
- Cavaleri, L., Sclavo, M., 2006. The calibration of wind and wave model data in the Mediterranean Sea. *Coastal Engineering* 53, 613–627.
- Chun, H., Suh, K., 2018. Estimation of significant wave period from wave spectrum, *Ocean Engineering* 163, 609–616.
- Datawell., 2009. Datawell Waverider Reference Manual, Datawell BV oceanographic instruments, The Netherlands, pp 123.
- Dean, R.G., Dalrymple, R., 1991. *Water Wave Mechanics for Engineers and Scientists*. World Scientific Publishing Ltd., Singapore
- DNV, 2000. DNV Classification Note 30.5 "Environmental conditions and environmental loads", DNV, Norway
- DNV, 2010. Recommended Practice DNV-RP-C205, October 2010, DNV, Norway
- Findlater, J., 1969. A major low-level air current near the Indian Ocean during the northern summer. *Quart. J. Roy. Meteor. Soc.* 95(404), 362-380. doi:[10.1002/qj.49709540409](https://doi.org/10.1002/qj.49709540409).
- Fonseca, N., Guedes Soares, C., 2003. Experimental investigation of the shipping of water on the bow of a containership, Proceedings of the 22 International Conference on Offshore Mechanics and Arctic Engineering (OMAE'03), 8-13 June, Cancun, Mexico, ASME, New York, Paper OMAE2003-37456.
- Glejin, J., Kumar, V.S, Anoop, T.R., Joseph, J., 2016. Directional characteristics of shallow water waves along south western Bay of Bengal, *Ocean Engineering* 121, 546-558. doi:[10.1016/j.oceaneng.2016.06.006](https://doi.org/10.1016/j.oceaneng.2016.06.006).
- Goda, Y., 1970. Numerical experiments on wave statistics with spectral simulation. Technical Note of the Port and Harbour Research Institute, Ministry of Transport. pp. 3–57 Japan, No.9.
- Goda, Y., 2010. *Random Seas and Design of Maritime Structures*, Third Edition, World Scientific Inc., Singapore.
- Haver, S., 2001. Evidences of the existence of freak waves, *Rogue Waves*, M. Olagnon and G. Atanassoulis, Eds, 129-140.
- Hithin, N.K., Kumar, V.S, Shanas, P.R., 2015. Trends of wave height and period in the Central Arabian Sea from 1996 to 2012: A study based on satellite altimeter data. *Ocean Engineering* 108, 416-425. doi: [10.1016/j.oceaneng.2015.08.024](https://doi.org/10.1016/j.oceaneng.2015.08.024).
- Holthuijsen, L.H., 2007. *Waves in Oceanic and Coastal Waters*, Cambridge University Press, Cambridge

- Huang, N.E., Shen, Z., Long, S.R., Wu, M.C., Shih, H.H., Zheng, Q., Yen, N.C., Tung, C.C., Liu, H.H., 1998. The empirical mode decomposition and the Hilbert spectrum for nonlinear and non-stationary time series analysis. *Proceedings of the Royal Society of London. Series A: Mathematical, Physical and Engineering Sciences* 454, 903-995.
- Kraus, N.C., Larson, M., 1988. Beach Profile Change Measured in the Tank for Large Waves 1956-1957 and 1962. Technical Report CERC-88-6.
- Kumar, D., Sannasiraj, S.A., Sundar, V., Polnikov, V.G., 2013. Wind-Wave Characteristics and Climate Variability in the Indian Ocean Region Using Altimeter Data. *Marine Geodesy* 36(3), 303-318.
- Kumar, V.S, Shanas, P.R., Dubhashi, K.K., 2014. Shallow water wave spectral characteristics along the eastern Arabian Sea, *Natural Hazards* 70, 377–394, doi: 10.1007/s11069-013-0815-7.
- Kumar, V.S, Kumar, K.A., Anand, N.M., 2000, Characteristics of waves off Goa, West coast of India, *Journal of Coastal Research*, 16(3), 782-789, www.jstor.org/stable/4300088
- Longuet-Higgins, M.S., 1983. On the joint distribution of wave periods and amplitudes in a random wave field. *Proceedings of the Royal Society of London. A. Mathematical and Physical Sciences* 389 (1797), 241-258.
- Longuet-Higgins, M. S., 1975. On the joint distribution of the periods and amplitudes of sea waves. *J. Geophys. Res.* 80(18), 2688-2694.
- Mandal, S., Nair, M.A., Kumar, V.S., 2020. Hilbert-Huang transform analysis of surface wavefield under tropical cyclone Hudhud. *Applied Ocean Research* 101, 102269. <https://doi.org/10.1016/j.apor.2020.102269>.
- Mendes, D., Oliveira, T.C.A., 2021. Deep-water spectral wave steepness offshore mainland Portugal, *Ocean Engineering*, 236, 109548, <https://doi.org/10.1016/j.oceaneng.2021.109548>.
- Mori, N., Janssen, P.A.E.M., 2006. On kurtosis and occurrence probability of freak waves. *Journal of Physical Oceanography* 36, 1471–1483.
- Myrhaug, D., 2018. Some probabilistic properties of deep-water wave steepness, *Oceanologia*, 60, 187-192, <https://doi.org/10.1016/j.oceano.2017.10.003>.
- Pecher, A., Kofoed, J.P., 2017. *Handbook of Ocean Wave Energy*; Springer International Publishing: Cham, Switzerland, pp 1-15. DOI 10.1007/978-3-319-39889-1.
- Sandhya, K.G., Balakrishnan Nair T.M., Bhaskaran, P.K., Sabique, L., Arun, N., Jeykumar, K., 2014. Wave forecasting system for operational use and its validation at coastal Puducherry, east coast of India. *Ocean Engineering* 80, 64-72.
- Schott, F., McCreary, J.P., 2001. The Monsoon Circulation of the Indian Ocean. *Progress Oceanography* 51, 1-123, [https://doi.org/10.1016/S0079-6611\(01\)00083-0](https://doi.org/10.1016/S0079-6611(01)00083-0).
- Semedo, A., Sušelj, K., Rutgersson, A., Sterl, A., 2011. A global view on the wind sea and swell climate and variability from ERA-40. *Journal of Climate* 24, 1461–1479, doi: 10.1175/2010JCLI3718.1.

- Smith, O.E., Adelfang, S.I., Tubbs, J.D., 1982. A bivariate gamma probability distribution with application to gust modeling (No. NASA-TM-82483). NASA Technical Memorandum, NASA Marshall Space Flight Center Huntsville, United States.
- Smith, G. H., Venugopal, V., Wolfram, J., 2006. Wave period group statistics for real sea waves and wave energy extraction. *Proceedings of the Institution of Mechanical Engineers, Part M: Journal of Engineering for the Maritime Environment*, 220(3), 99-115.
- Stokes, G.G., 1880. Supplement to a paper on the theory of oscillatory waves, *Mathematical and Physical Papers*, Vol.1, Cambridge University Press, London, 314-326.
- Taylor, P.K., Yelland, M.J., 2001. The dependence of sea surface roughness on the height and steepness of the waves. *J. Physical Oceanography* 31, 572-590.
- Teutsch, I., Weisse, R., Moeller, J., and Krueger, O., 2020. A statistical analysis of rogue waves in the southern North Sea, *Nat. Hazards Earth Syst. Sci.*, 20, 2665–2680, <https://doi.org/10.5194/nhess-20-2665-2020>.
- Thompson, W. C., Nelson, A. R., Sedivy, D. G., 1984. Wave group anatomy of ocean wave spectra, *Proceeding of 19th conference on Coastal engineering*, American Society of Civil Engineers, 1, 661–677.
- Toffoli, A., Lefever, J.M., Bitner-Gregersen, E., Monbaliu, J., 2005. Towards the identification of warning criteria: analysis of a ship accident database. *Appl. Ocean Res.* 27, 281–291. <https://doi.org/10.1016/j.apor.2006.03.003>.
- Tucker, M.J., 1991. *Waves in ocean engineering: measurement, analysis, interpretation*. Ellis Horwood, Chichester, UK. 431 pp.
- Tucker, M.J., Pitt, E.G., 2001. *Waves in ocean engineering*, Elsevier, Amsterdam. p548.
- Vinoth, J., Young, I.R., 2011. Global estimates of extreme wind speed and wave height. *Journal of Climate*, 24, 1647-1665. doi: 10.1175/2010JCLI3680.1.
- Wu, C. H., Yao, A., 2004. Laboratory measurements of limiting freak waves on currents, *J. Geophys. Res.*, 109, C12002, doi:10.1029/2004JC002612.
- Xinran Ji, Aiping Li, Jixuan Li, Lei Wang, Daoru Wang, 2022. Research on the statistical characteristic of freak waves based on observed wave data, *Ocean Engineering*, 243, 110323, <https://doi.org/10.1016/j.oceaneng.2021.110323>.

Annexure. Notations and definition of wave parameters used in the study

H = individual wave height

d = water depth at the measurement location

T = individual wave period

L = wavelength at the measurement location of individual wave estimated as per dispersion relationship from period

k = wave number = $2\pi/L$

L_m = wavelength estimated from the mean wave period (T_{m02})

L_p = wavelength estimated from the peak wave period (T_p)

δ - steepness of individual wave = H/L

$\langle\delta\rangle$ = average wave steepness of waves in a wave record of 30-minutes

H^* = normalized wave height = $H/\sqrt{m_0}$

δ^* = normalized wave steepness = $\delta \frac{L_m}{H_m}$

GPR = Group power ratio = group energy/time group length

Significant wave steepness (δ_m) = H_s/L_m

Significant wave steepness (δ_p) = H_s/L_p

$H_{1/3}$ = significant wave height = the average of the highest 1/3rd waves in in a 30-minutes record obtained from zero-up-crossing analysis

$T_{1/3}$ = significant wave period

H_{max} = maximum height of the wave in a 30-minutes duration

H_s = significant wave height = $4\sqrt{m_0}$ (A1)

T_e = energy wave period = $\frac{m_{-1}}{m_0}$ (A2)

T_{m02} = mean wave period = $\sqrt{\frac{m_0}{m_2}}$ (A3)

$T_{m-1,1}$ = average wave period = $\sqrt{\frac{m_{-1}}{m_1}}$ (A4)

Spectral width parameter = $\sqrt{\frac{m_2 m_0 - m_1^2}{m_1^2}}$ (A5)

where m_n is the nth order spectral moment and given by $m_n = \int_0^\infty f^n S(f) df$, $n=0$ and -1 , and $S(f)$ is the spectral energy density at frequency f .

Table 1. Locations considered in the study and the annual average wave heights

Location	Position	Water depth (m)	Period of data used	Data (%)	Annual average H_s (m)	Annual average H_{max} (m)	Number of waves
Versova	19.130° N; 72.740° E	10	1 January 2017-31 December 2017	99.99	0.91	1.38	6417657
Ratnagiri	16.980° N; 73.258° E	13	1 January 2017-31 December 2017	99.98	1.14	1.73	5872581
Vengurla	15.842° N 73.563° E	15	1 January 2017-31 December 2017	99.99	0.98	1.51	5597770
Karwar	14.822° N; 74.052° E	15	1 January 2017-31 December 2017	99.46	1.13	1.76	5497168

Table 2. Maximum value of crest height, trough height and wave height in different months at Versova, Ratnagiri, Vengurla and Karwar.

Highest values are indicated in bold letters

Month	Versova			Ratnagiri			Vengurla			Karwar		
	Crest height (m)	Trough height (m)	Wave height (m)	Crest height (m)	Trough height (m)	Wave height (m)	Crest height (m)	Trough height (m)	Wave height (m)	Crest height (m)	Trough height (m)	Wave height (m)
Jan	1.48	1.10	2.29	1.74	1.34	2.87	1.10	1.03	1.70	1.35	1.13	2.15
Feb	1.55	1.18	2.51	1.85	2.13	3.06	1.38	1.20	2.32	1.76	1.63	2.92
Mar	1.22	1.36	2.37	1.32	1.29	2.29	1.14	1.11	1.90	1.34	1.04	2.12
Apr	1.24	1.13	2.28	1.31	1.19	2.37	1.24	1.00	1.98	1.34	1.30	2.14
May	2.16	1.73	3.46	2.95	2.59	4.83	2.71	1.99	4.38	2.77	2.24	4.97
Jun	4.06	2.66	5.74	4.32	3.46	6.95	4.45	2.87	7.28	4.36	3.35	6.70
Jul	3.97	2.33	5.64	4.47	3.42	6.83	4.08	2.99	5.98	4.80	3.57	7.61
Aug	3.26	2.75	5.52	3.81	2.68	5.85	2.96	2.23	4.66	3.04	2.60	5.12
Sep	3.10	2.27	4.83	3.27	2.72	5.87	3.17	2.38	4.85	3.01	2.51	4.77
Oct	0.99	0.94	1.75	1.09	0.94	1.86	0.93	0.84	1.51	1.16	1.14	1.88
Nov	1.16	0.97	2.01	1.05	0.94	1.80	0.86	0.71	1.57	0.88	0.86	1.58
Dec	2.21	1.83	3.76	2.86	2.40	4.78	2.90	2.29	4.41	2.49	2.35	4.00

Table 3. Percentage of short-period, long-period and intermediate-period waves in different seasons at Versova, Ratnagiri, Vengurla and Karwar and their mean wave height

Location	Season	Percentage			Mean wave height (m)		
		short-period	long-period	intermediate-period	short-period	long-period	intermediate-period
Versova	Feb-May	82.5	5.6	11.9	0.38	0.52	0.51
	Jun-Sep	53.2	27.2	19.6	0.59	1.25	1.00
	Oct-Jan	80.6	9.4	10.0	0.27	0.38	0.34
	Jan-Dec	72.0	14.1	13.9	0.41	0.72	0.62
Ratnagiri	Feb-May	75.1	9.5	15.4	0.42	0.63	0.57
	Jun-Sep	44.7	31.4	23.9	0.71	1.55	1.25
	Oct-Jan	76.0	9.8	14.2	0.32	0.48	0.43
	Jan-Dec	65.2	16.9	17.8	0.48	0.89	0.75
Vengurla	Feb-May	68.3	16.4	15.3	0.25	0.44	0.36
	Jun-Sep	40.9	36.3	22.8	0.61	1.42	1.09
	Oct-Jan	72.1	13.3	14.6	0.31	0.55	0.46
	Jan-Dec	60.4	22.0	17.6	0.39	0.80	0.64
Karwar	Feb-May	68.8	14.8	16.4	0.37	0.64	0.54
	Jun-Sep	41.1	35.3	23.6	0.69	1.58	1.24
	Oct-Jan	69.0	14.8	16.2	0.32	0.55	0.46
	Jan-Dec	59.6	21.7	18.8	0.46	0.93	0.75

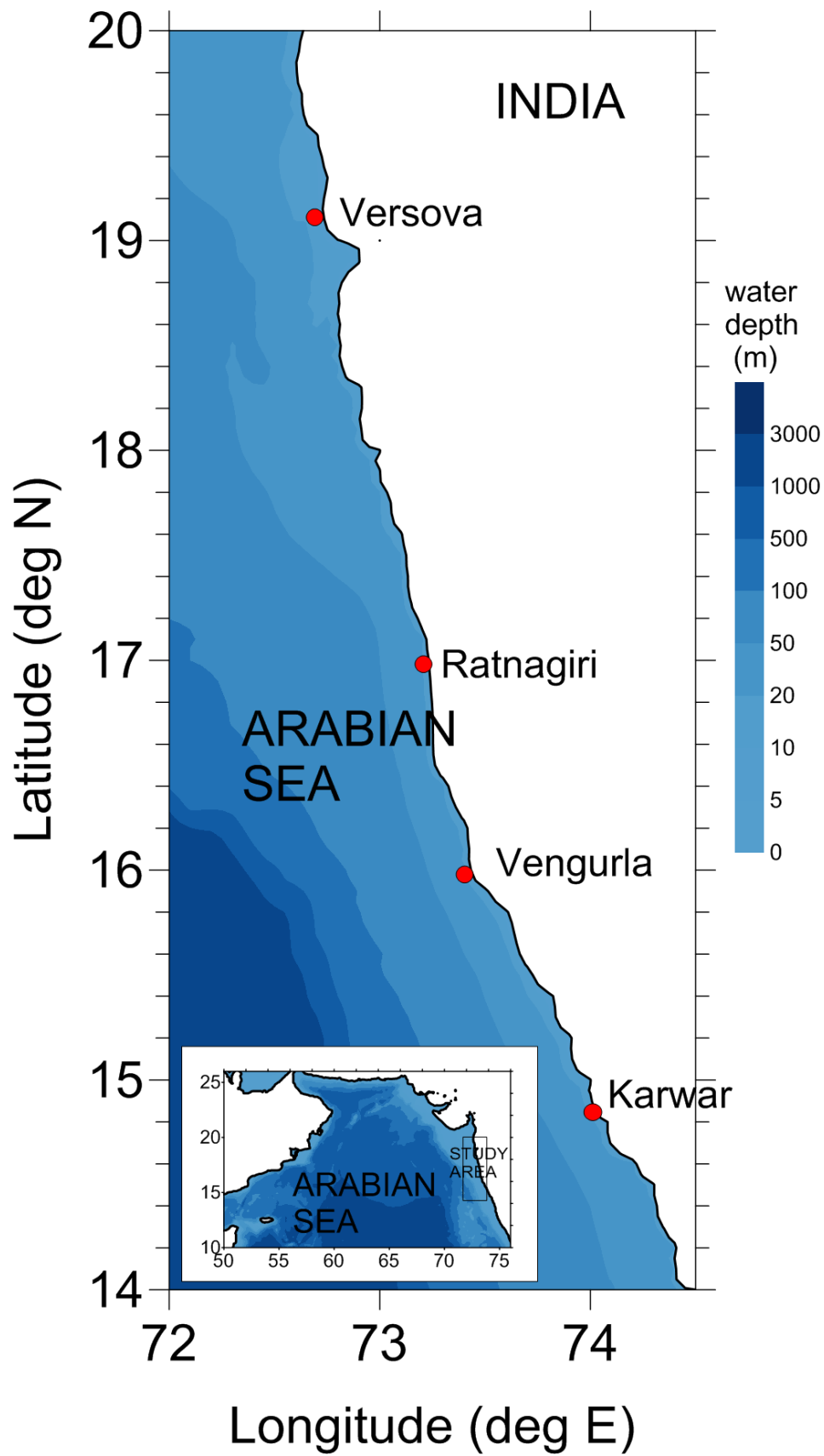


Figure 1. Map showing the geographical locations of Waverider buoy and the study area in the eastern Arabian Sea. Contour level indicates the water depth

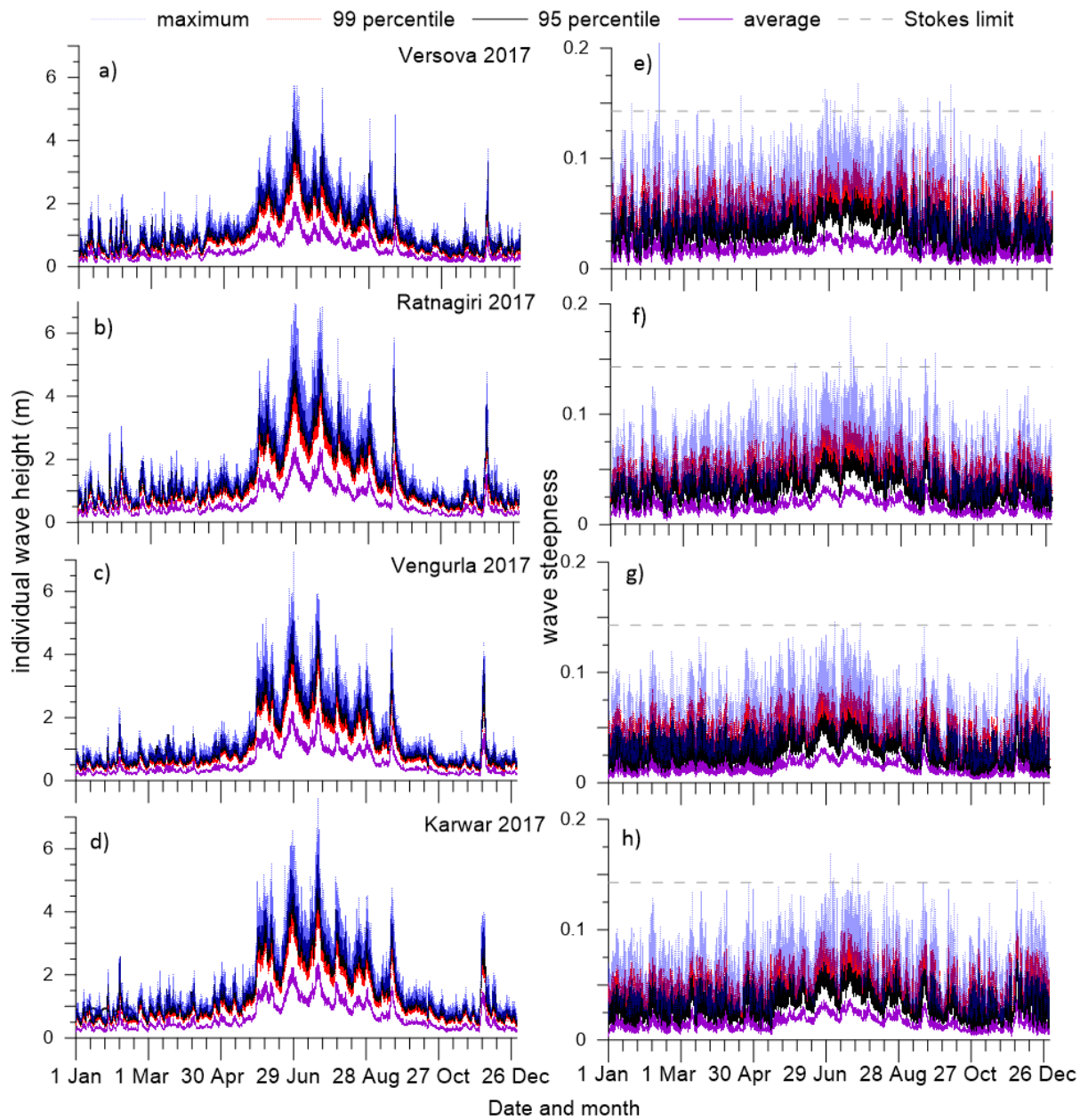


Figure 2. Left panel shows the time series plot of height statistics (maximum, 99th percentile, 95th percentile and average) of individual waves at every 30 minutes interval from 1 January to 31 December 2017 at a) Versova, b) Ratnagiri, c) Vengurla, and d) Karwar. Right panel shows the time series plot of wave steepness statistics of individual waves at every 30 minutes interval during 2017 at e) Versova, f) Ratnagiri, g) Vengurla, and h) Karwar

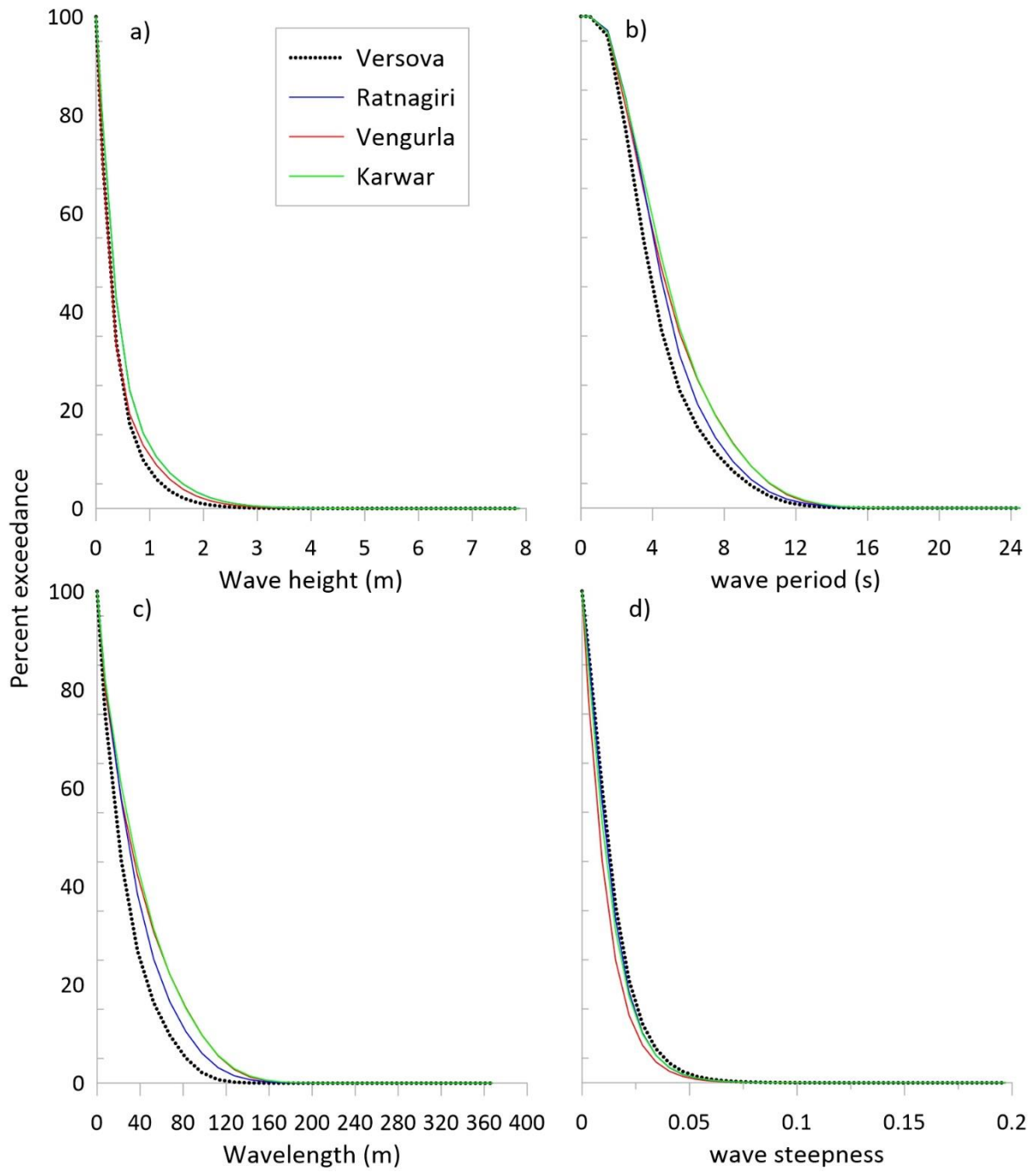


Figure 3. Percent exceedance of a) height, b) period, c) length and d) steepness of individual waves measured in 2017 at Versova, Ratnagiri, Vengurla, and Karwar

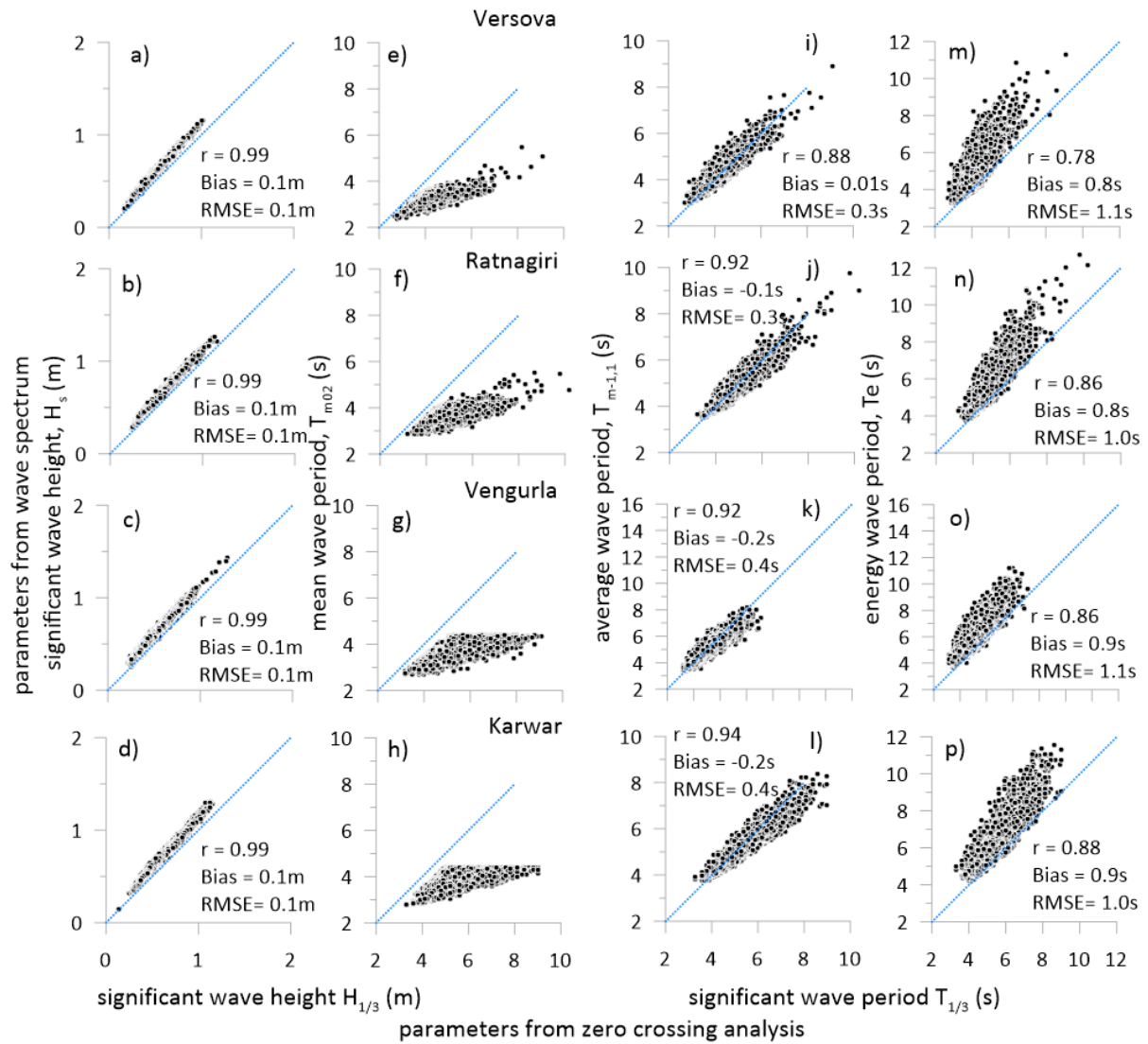


Figure 4. Scatter plots of wave parameters obtained from zero-up-crossing analysis and wave spectrum. a to d is significant wave height, e to h is mean wave period (T_{m02}) and significant wave period, i to l is average wave period ($T_{m-1,1}$) and significant wave period, m to p is energy wave period ($T_{m-1,0}$) and significant wave period. Solid line is the exact match line. At all locations deep-water waves are only used in the plots.

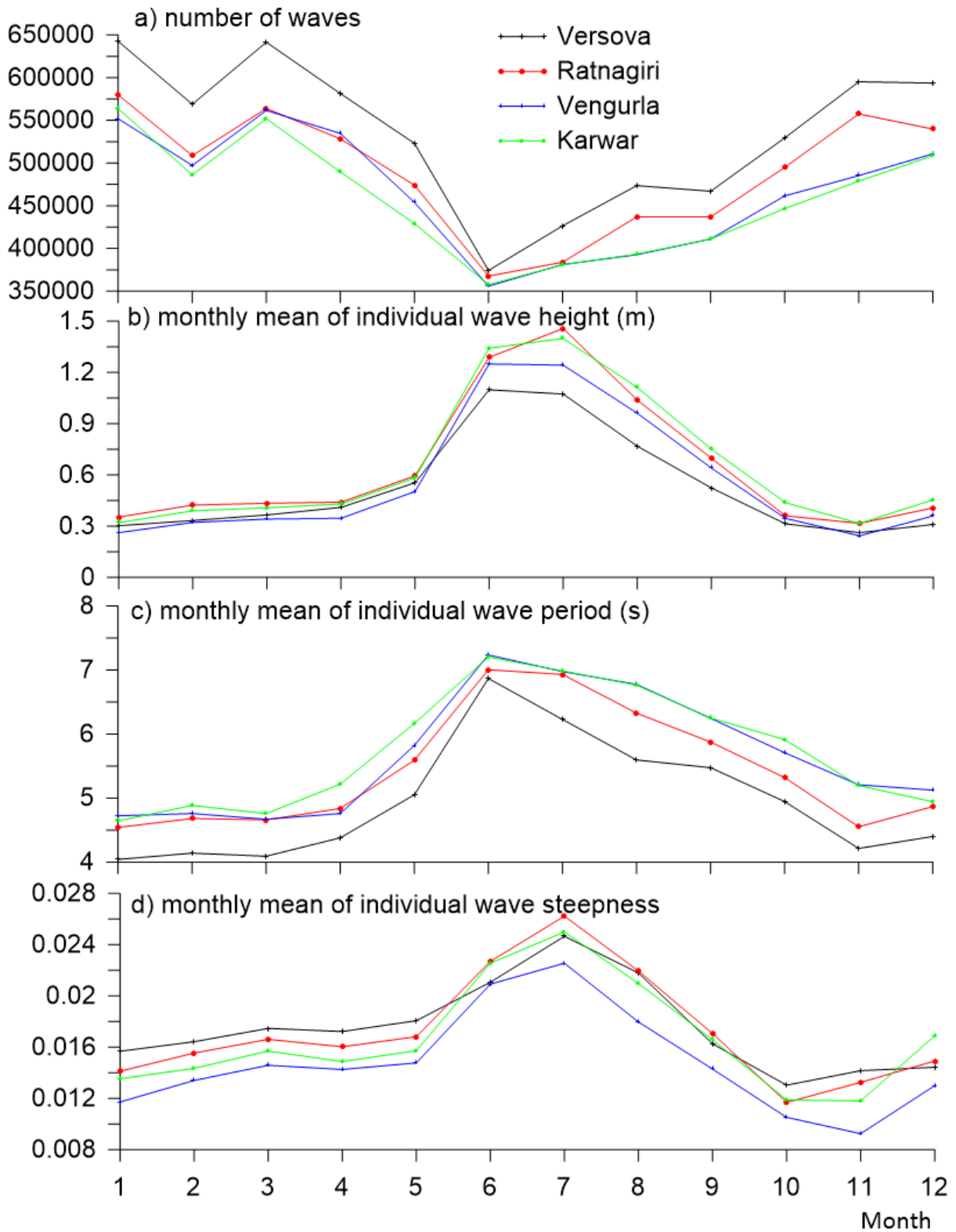


Figure 5. Plots of a) total number of waves measured in different months, b) monthly mean of individual wave height, c) monthly mean of individual wave period and d) monthly mean of individual wave steepness

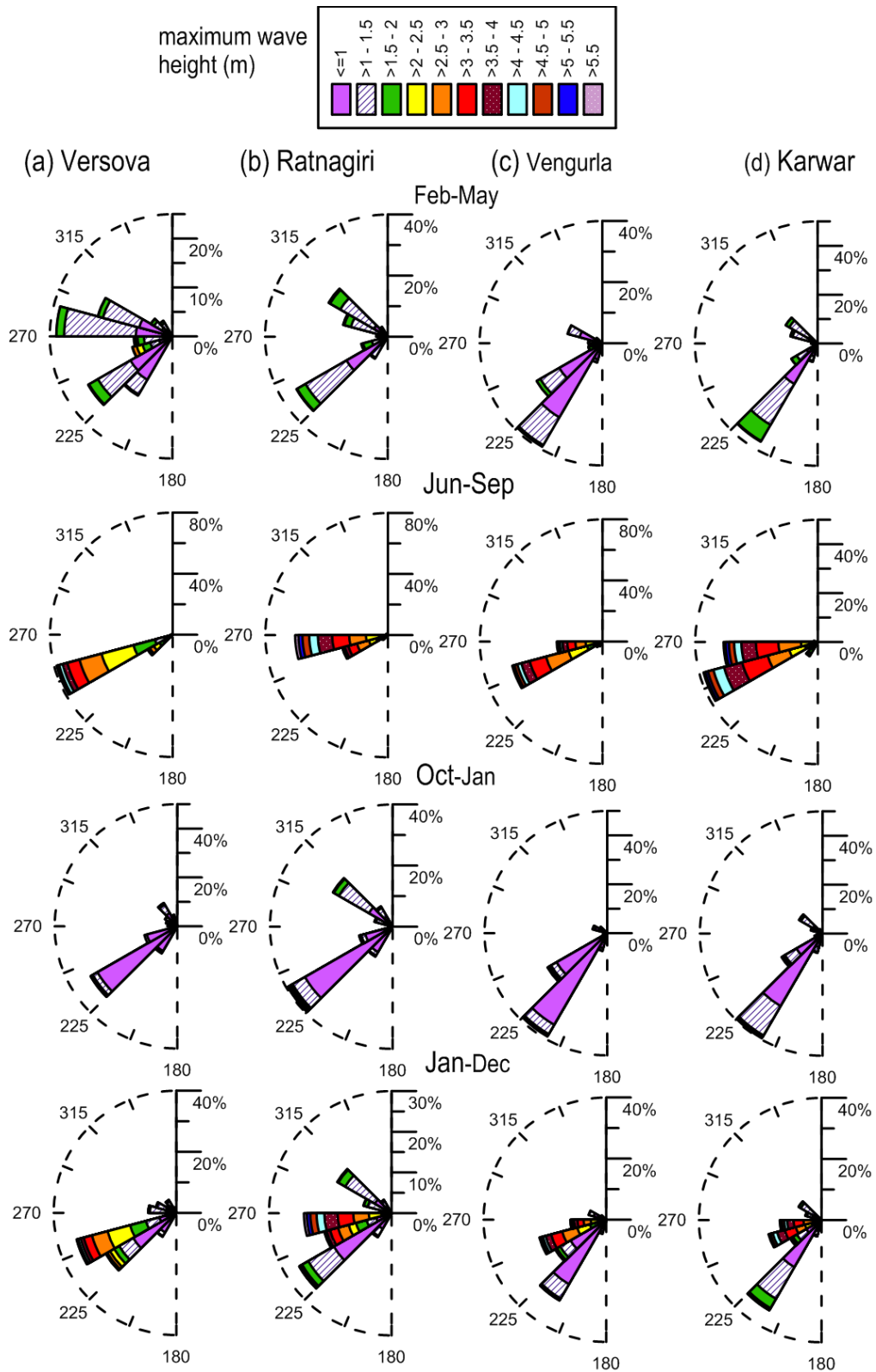


Figure 6. Wave roses (maximum wave height and mean wave direction) during different periods from 1 January 2017 to 31 December 2017 at different locations. (a) Versova, (b) Ratnagiri, (c) Vengurla, (d) Karwar. The plots represent the direction where the waves come from. The radius of the figure indicates the percentage of the time

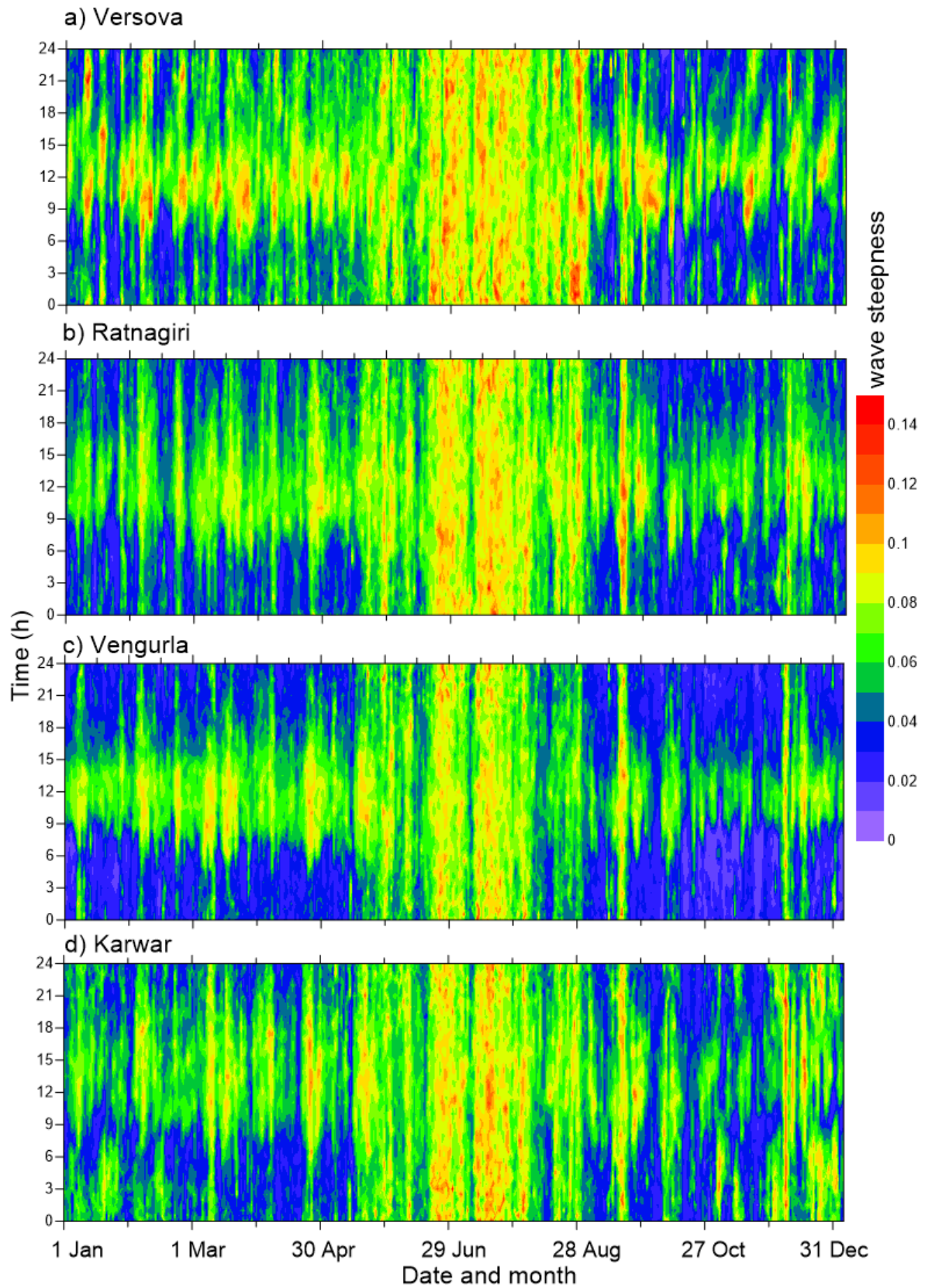


Figure 7. Temporal distribution of maximum steepness in 2017 at all the four study locations

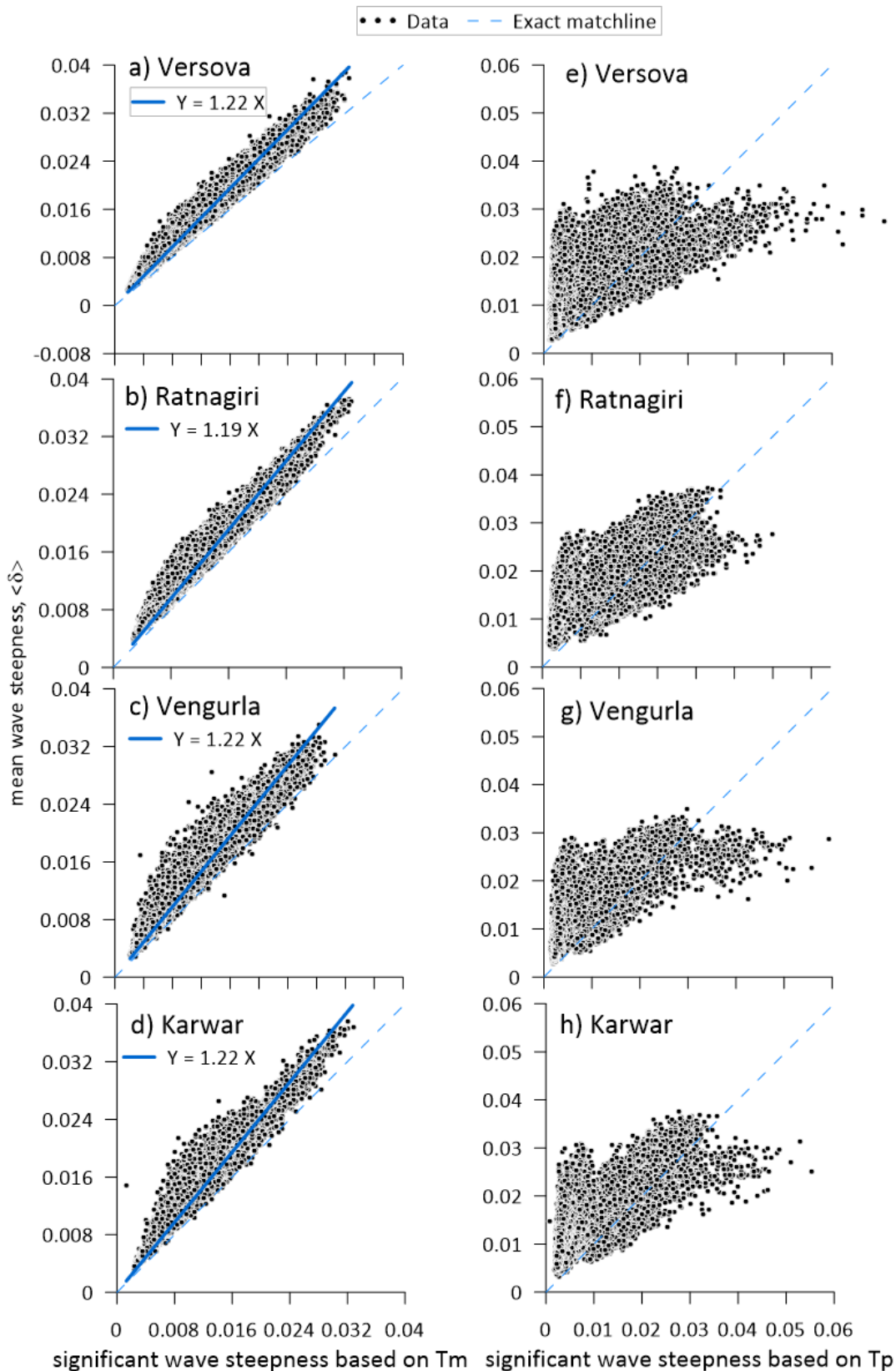


Figure 8.a to d) Scatter diagrams for mean wave steepness of 30-minutes record and the corresponding significant wave steepness based on mean wave period. e to h) between mean wave steepness and significant wave steepness based on peak wave period at the 4 locations of study

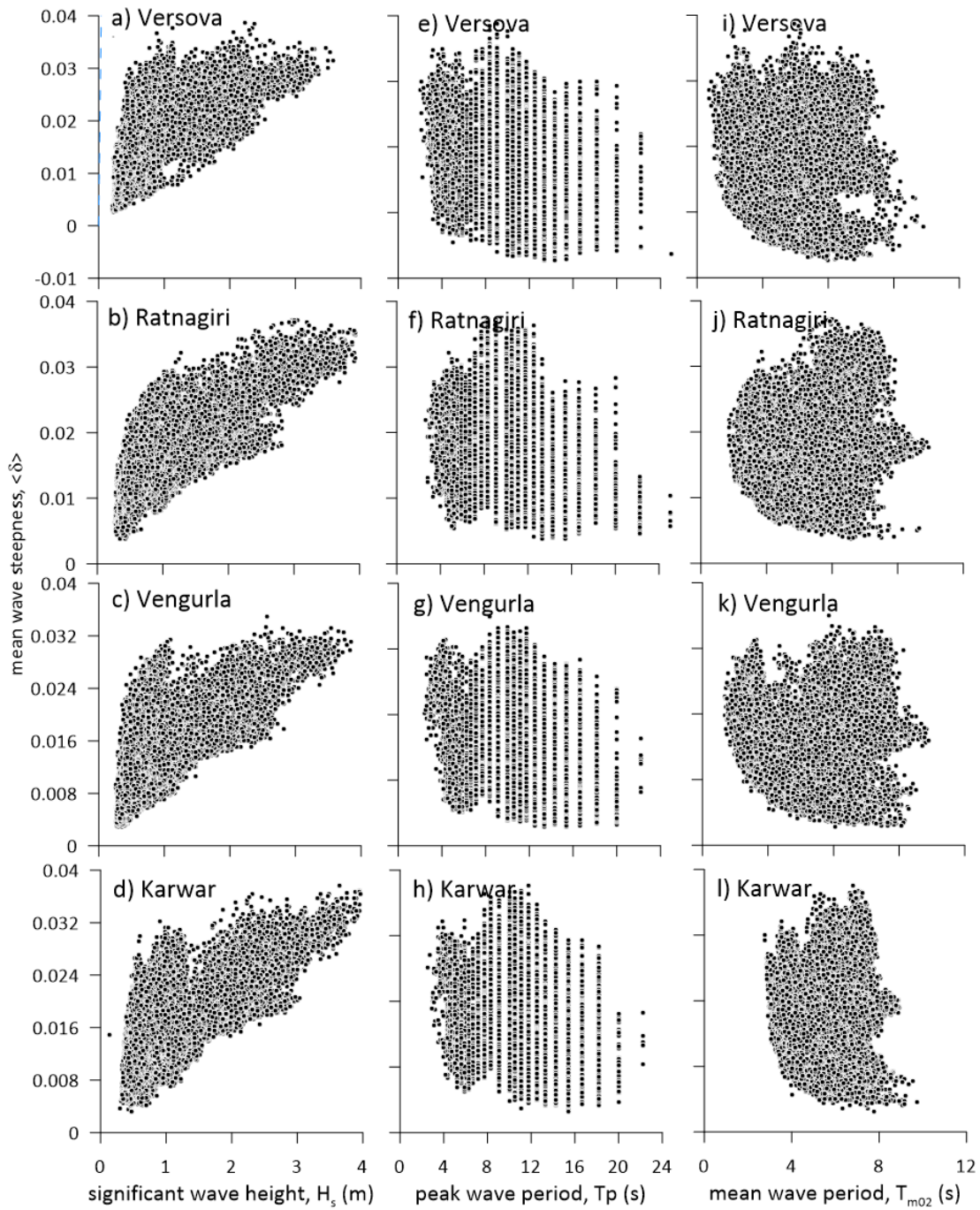


Figure 9. Variation of mean wave steepness with significant wave height (a to d), peak wave period (e to h) and mean wave period (i to l)

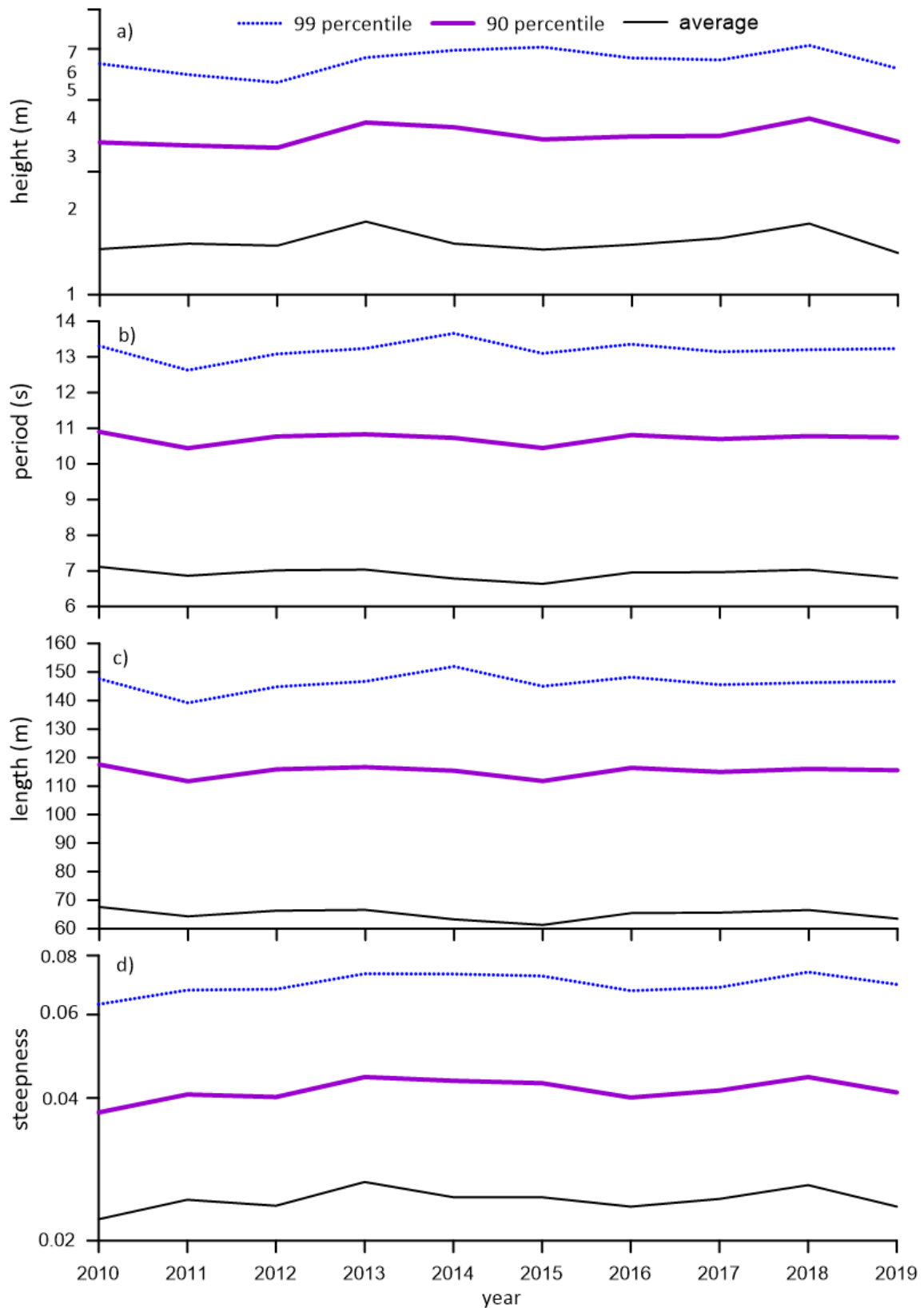


Figure 10. 99 percentile, 90 percentile and average value of a) height, b) period, c) length and d) steepness of individual waves measured in June and July of different years at Ratnagiri

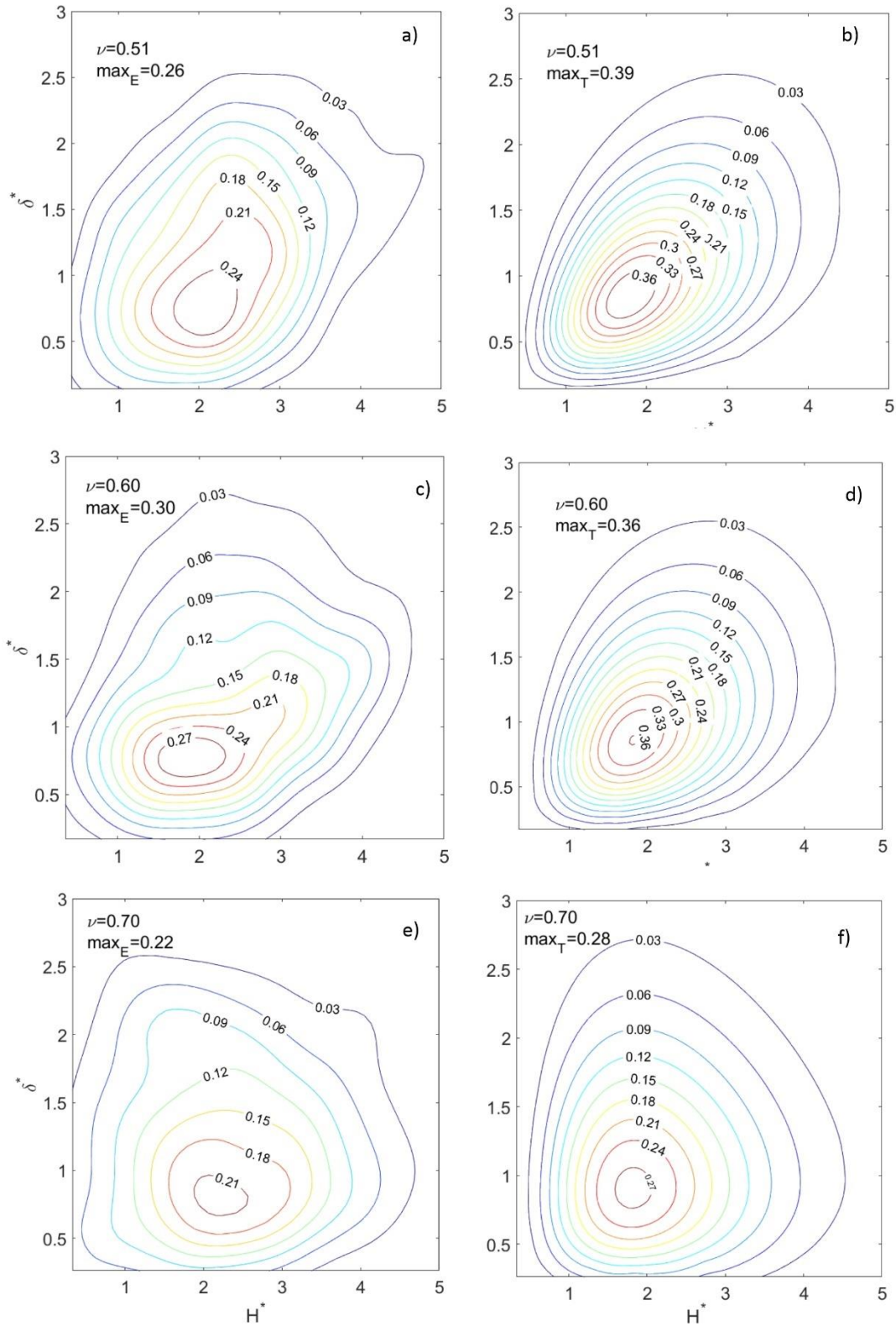


Figure 11. Joint probability density of normalized wave height and steepness for different spectral width parameter $\nu =$ (a) 0.51, (c) 0.60 and (e) 0.70 based on data measured at Ratnagiri. Empirical and theoretical joint probability density are presented in right and left column respectively

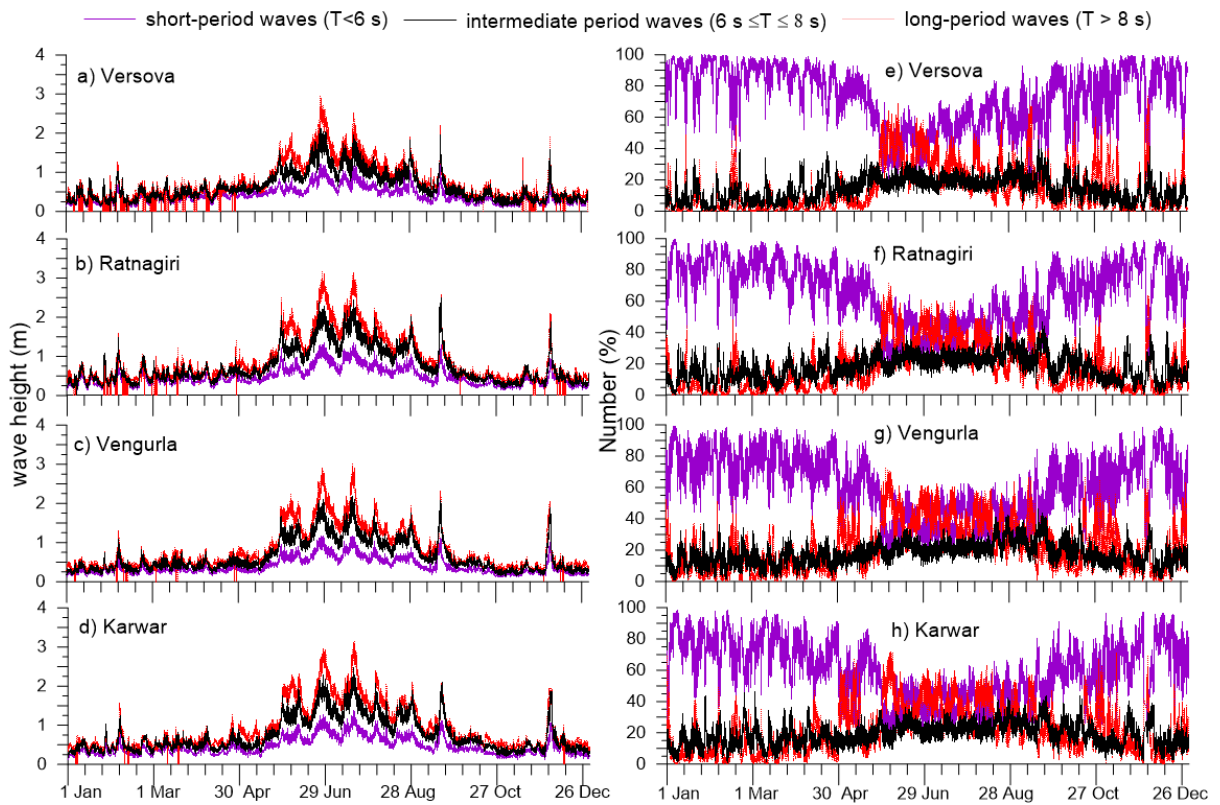


Figure 12. Distribution of short-period, intermediate-period and long-period waves at different locations. a to d shows the time series plot of average wave height of short-period, intermediate-period and long-period waves in each 30 minutes record during 1 January to 31 December 2017 and e to f is the corresponding percentage

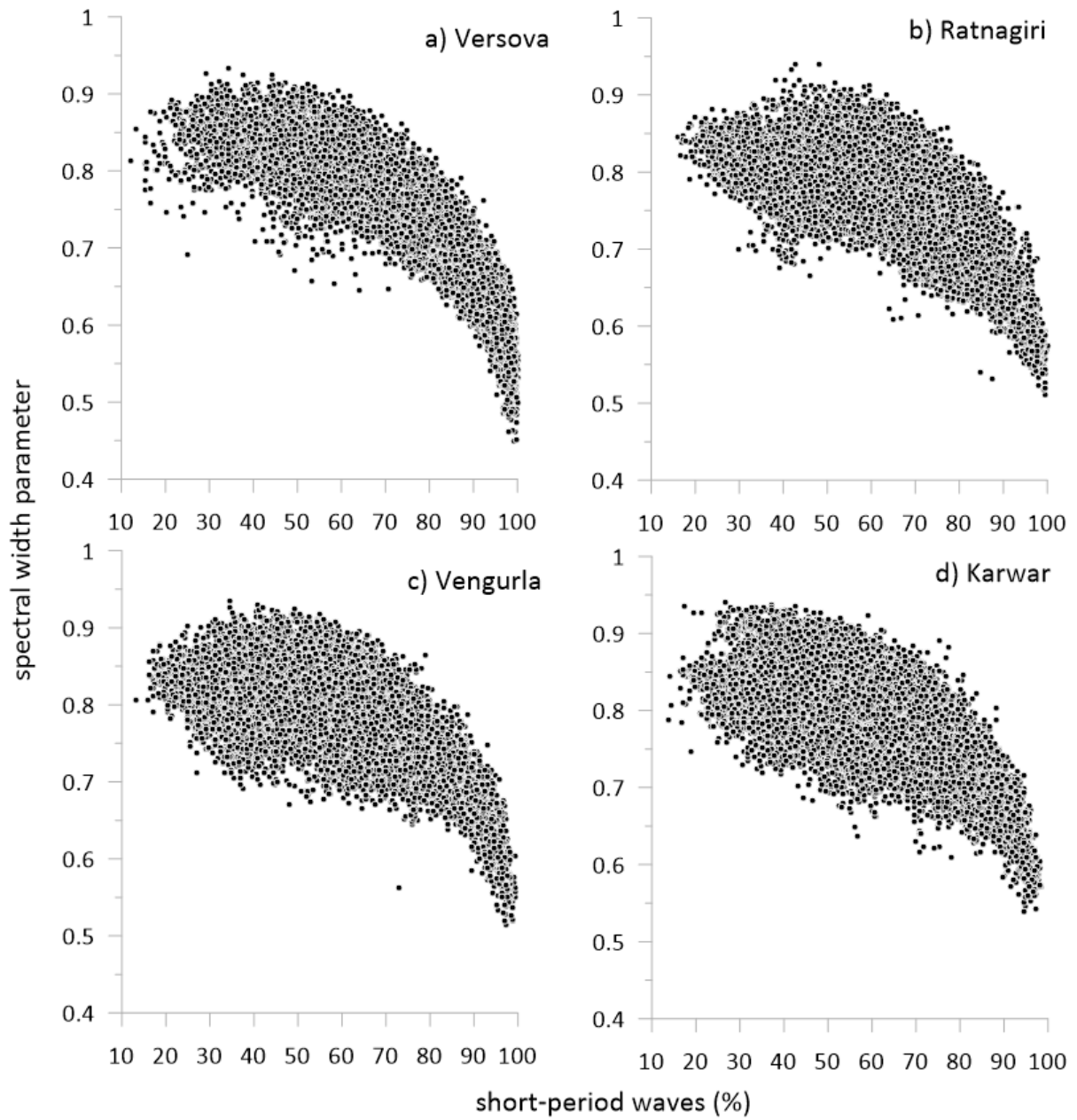


Figure 13. Scatter plots of percentage of short-period waves with spectral width parameter

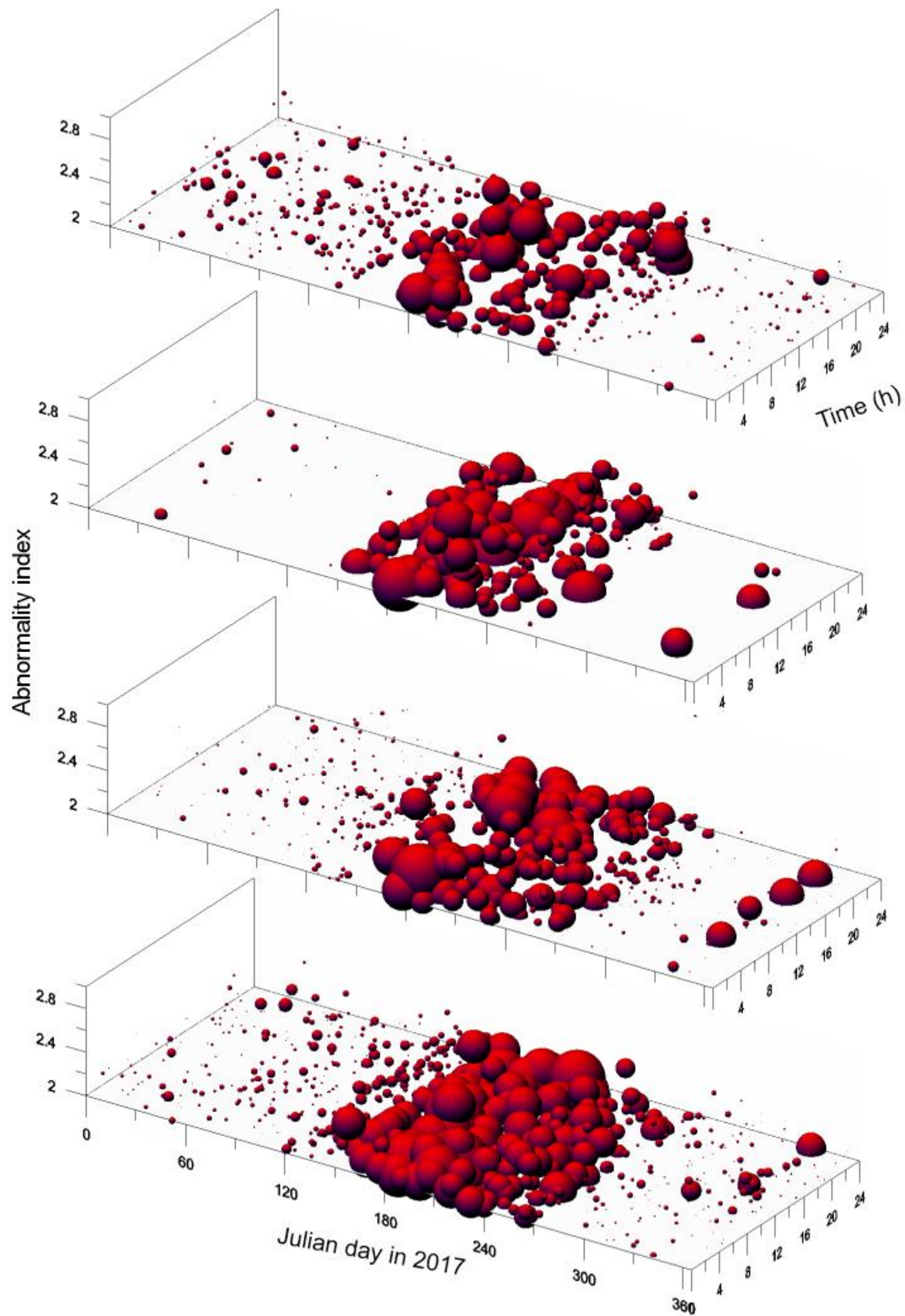


Figure 14. Distribution of freak waves and its height at different locations in 2017. The size of the bubble is the significant wave height, which vary from 0.5 to 4 m. Vertical axis is the abnormality index. From top to bottom, locations are Versova, Ratnagiri, Vengurla and Karwar

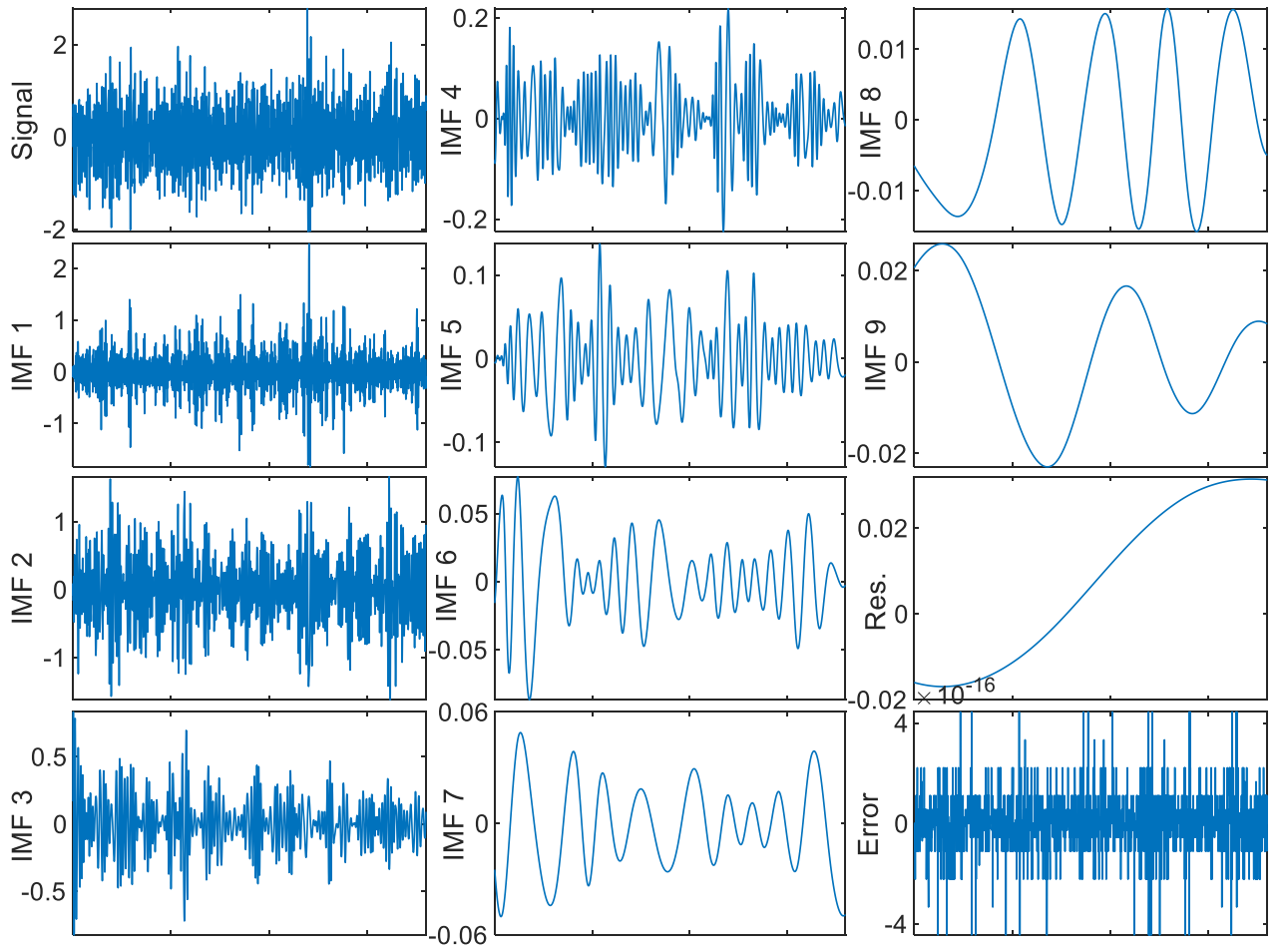


Figure 15. Decomposition of wave record A2 by Empirical Mode Decomposition

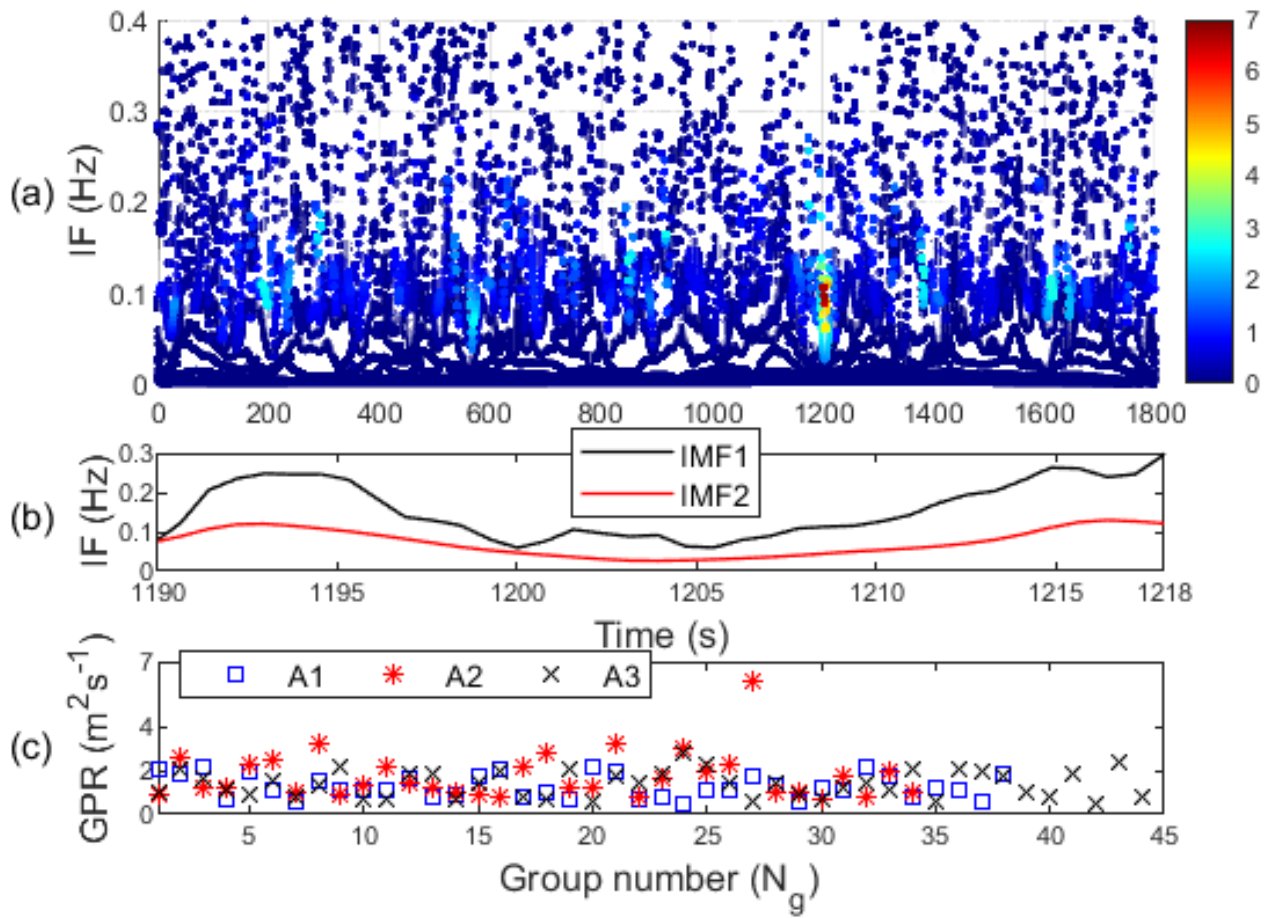


Figure 16. (a) Instantaneous energy spectrum for A2, (b) time variations of instantaneous frequency (IF) of IMF1 and IMF2 and (c) group power ratio (GPR) (E_{gl}/t_g) vs Group number (N_g) for A1, A2 and A3

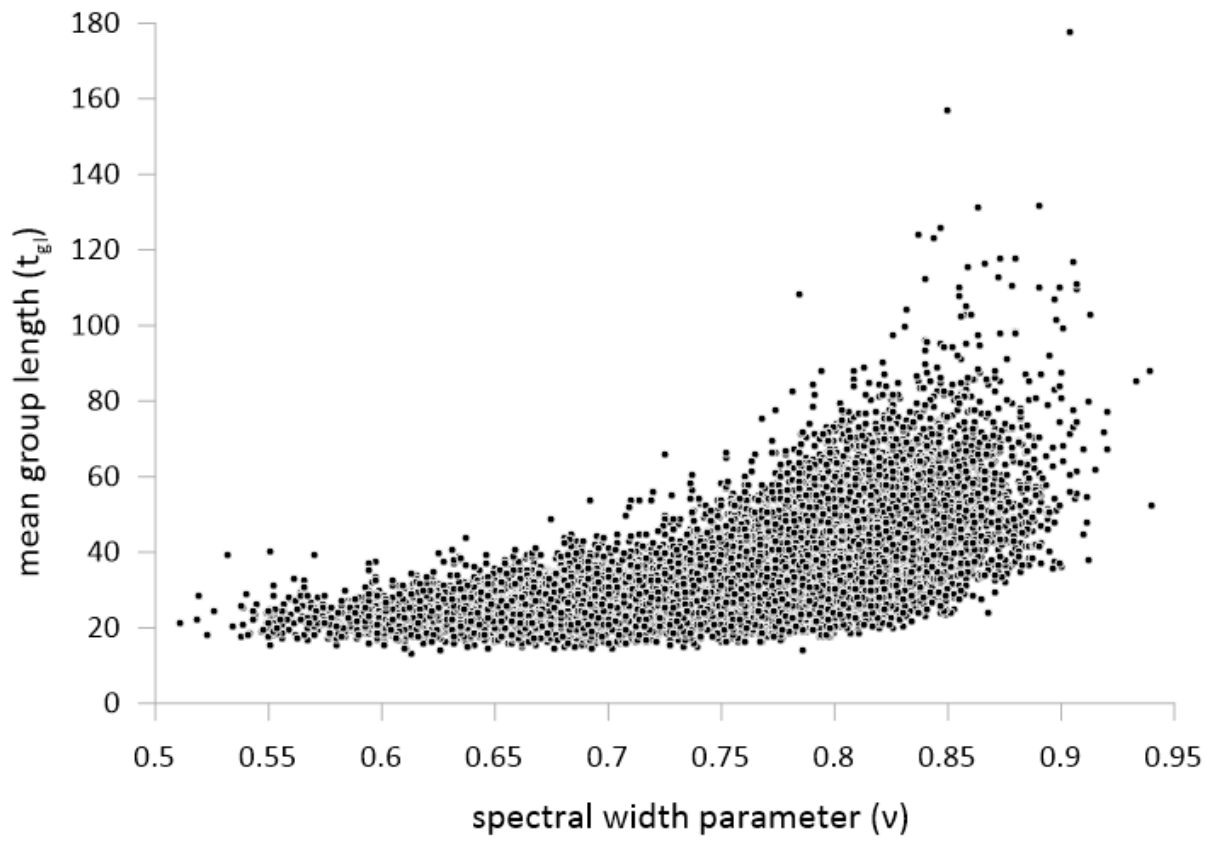


Figure 17. Variation of mean group length ($\overline{t_{gl}}$) with spectral width parameter (ν) for one-year wave record at Ratnagiri